Time Markers for the Evolution and Exhumation History of a Late Palaeozoic Paired Metamorphic Belt in North–Central Chile (34°–35°30′S)

ARNE P. WILLNER[1]*, STUART N. THOMSON[1,2], ALFRED KRÖNER[3], JO-ANNE WARTHO[4], JAN R. WIJBRANS[5] AND FRANCISCO HERVÉ[6]

[1]INSTITUT FÜR GEOLOGIE, MINERALOGIE UND GEOPHYSIK, RUHR-UNIVERSITÄT, D-44780 BOCHUM, GERMANY

[2]DEPARTMENT OF GEOLOGY AND GEOPHYSICS, YALE UNIVERSITY, P.O. BOX 208109, NEW HAVEN, CT 06520-8109, USA

[3]INSTITUT FÜR GEOWISSENSCHAFTEN, UNIVERSITÄT MAINZ, BECHERWEG 21, D-55099 MAINZ, GERMANY

[4]WESTERN AUSTRALIAN ARGON ISOTOPE FACILITY, DEPARTMENT OF APPLIED GEOLOGY, CURTIN UNIVERSITY OF TECHNOLOGY, HAYMAN ROAD, BENTLEY, W.A. 6102, AUSTRALIA

[5]FACULTEIT DER AARDWETENSCHAPPEN, VRIJE UNIVERSITEIT AMSTERDAM, DE BOELELAAN 1085, 1081 HV AMSTERDAM, THE NETHERLANDS

[6]DEPARTAMENTO DE GEOLOGIA, UNIVERSIDAD DE CHILE, CASILLA 13518, CORREO 21, SANTIAGO, CHILE

A multi-method geochronological approach is applied to unravel the dynamics of a paired metamorphic belt in the Coastal Cordillera of central Chile. This is represented by high-pressure–low-temperature rocks of an accretionary prism (Western Series), and a low-pressure–high-temperature overprint in the retro-wedge with less deformed metagreywackes (Eastern Series) intruded by magmas of the coeval arc. A pervasive transposition foliation formed in meta-greywackes and interlayered oceanic crust of the Western Series during basal accretion near metamorphic peak conditions ($\sim$350–400°C, 7–11 kbar) at 292–319 Ma ($^{40}Ar/^{39}Ar$ phengite plateau ages). $^{40}Ar/^{39}Ar$ UV laser ablation ages of phengite record strain-free grain growth and recrystallization with a duration of 31–41 Myr during a pressure release of 3–4 kbar. During early accretion the main intrusion in the arc occurred at 305 Ma (Pb–Pb evaporation; zircon) and the Eastern Series was overprinted by a short high-temperature metamorphism at 3 kbar, 296–301 Ma ($^{40}Ar/^{39}Ar$ muscovite plateau ages). Fission-track ages of zircon (206–232 Ma) and of apatite (80–113 Ma) are similar in both series, indicating synchronous cooling during distinct periods of exhumation. Early exhumation (period I) during continuing basal accretion proceeded with mean rates of $\geq$0·19–0·56 mm/yr, suggesting that erosion in a tectonically active area was an important

unroofing mechanism. At the same time mean rates were 0·03–0·05 mm/yr in the Eastern Series, where crustal thickening was minor. A shallow granite intruded into the Western Series at 224 Ma, at the end of basal accretion activity, when exhumation rates decreased to 0·04–0·06 mm/yr in both series during period II ($\sim$100–225 Ma). Major extension, basin formation and local bimodal dyke intrusion at 138 Ma were accompanied by mean cooling rates of $\sim$1–2°C/Myr. Accelerated cooling of 3–5°C/Myr at $\sim$80–113 Ma suggests a mid-Cretaceous convergence event (period III). After 80 Ma cooling rates decreased to 1–2°C/Myr (period IV). The pressure–temperature–deformation–time information for subduction, basal accretion and exhumation in the accretionary wedge of central Chile illustrates that these processes reflect a continuous cyclic mass flow that lasted nearly 100 Myr, while the retro-wedge remained stable. After the cessation of accretion activity a similarly long period of retreat of the subducting slab occurred; this ended with renewed convergence and shortening of the continental margin.

KEY WORDS: *exhumation rates; Ar/Ar geochronology; fission-track geochronology; Chile; paired metamorphic belt*

*Corresponding author. E-mail: arne.willner@ruhr-uni-bochum.de

INTRODUCTION

Exhumation mechanisms and rates in different geodynamic regimes have become a major focus of research in the past decade. Fossil accretionary prisms at convergent margins are key sites where high-pressure rocks are exhumed, and this process is related in time to activity in an associated magmatic arc. Circum-Pacific convergent margins are known for the occurrence of fossil paired metamorphic belts, i.e. HP–LT rocks within the accretionary wedge and LP–HT rocks within the magmatic arc (e.g. Ernst, 1975), that were not incorporated into later collisional orogens. If related processes within these paired belts can be proven, direct insights are provided into the dynamics of deep crustal levels of growing convergent margins. Along the South American convergent margin a paired metamorphic belt was first proposed by Aguirre *et al.* (1972) for the late Palaeozoic metamorphic basement of central Chile (Fig. 1). Although the contemporaneous nature of processes so far had only been indirectly inferred, this concept was successfully applied to most of the basement within the Chilean Coastal Cordillera between ∼26° and 55°S (Hervé, 1988).

Precise dating of the peak of high-pressure metamorphism and subsequent stages during exhumation along a well-understood pressure–temperature (*PT*) path is crucial for better understanding of the evolution and destruction of accretionary prisms and their duration in relation to the retro-wedge area and the magmatic arc. It has been demonstrated that the processes of subduction, exhumation, erosion and re-sedimentation, particularly in accretionary prisms, should represent a continuous material recycling system over a certain period of time (Cowan & Schilling, 1978; Gerya *et al.*, 2002; Kukowski *et al.*, 2002; Glodny *et al.*, 2005). However, the mechanisms that initiate, control and terminate subduction mass flow in accretionary prisms are as yet poorly understood, mainly because of a lack of time markers for the processes in detail.

The goal of this paper is to provide more information on the contemporaneity of processes, as well as on timing and rates of exhumation, in the fossil paired metamorphic belt of central Chile by applying a multi-method approach. We dated white mica using the ^{40}Ar/^{39}Ar technique to constrain the ages of the metamorphic peak in both the HP–LT and the LP–HT belts and to obtain information on the influence of deformation and fluid infiltration into the system during the early exhumation of rocks in the accretionary prism. Fission-track dating of zircon and apatite was applied to gain information on the late cooling paths, and hence on exhumation rates and mechanisms. The coeval magmatic events in the study area were dated based on selected granite samples using the Pb–Pb evaporation method. In an associated paper (Willner, 2005) related details of the *PT* evolution and reaction history in the rocks of both metamorphic belts have been presented.

The key questions to be addressed are: Which processes are contemporaneous in the paired metamorphic belt? Can the cyclic nature of the evolution of the accretionary prism be proven? When did accretion start and when did it finish? What processes are related to the beginning and the end of accretion? Can exhumation mechanisms be inferred from exhumation rates? What happened after the end of constructive processes such as accretion and intrusion in the paired metamorphic belt?

GEOLOGICAL SETTING AND PREVIOUSLY PUBLISHED AGE DATA

We studied the classic region between Pichilemu and Constitución in the central Chilean Coastal Cordillera (34°–35°30′S; Fig. 1; Table 1), where Aguirre *et al.* (1972) proposed a paired metamorphic belt and made the fundamental subdivision into two contrasting metamorphic complexes, the Western and Eastern Series. The Western Series represents the accretionary prism and is characterized by metagreywackes interlayered with lenses of oceanic crust. The latter consist of mainly greenschist, rare blueschist and associated Fe–Mn-rich metasediments, minor metachert and serpentinite. All these rocks are pervasively deformed and characterized by a second flat-lying transposition foliation, which formed close to and slightly after the peak of HP–LT metamorphism at ∼350–400°C and 7–11 kbar (Willner, 2005). This deformation represents mainly ductile thinning immediately following basal accretion. The subsequent early retrograde *PT* path is characterized by a pressure release of 3–4 kbar, followed by slight cooling with abundant recrystallization and continuing localized mineral growth, mainly under static conditions, and by the presence of abundant hydrous fluids. Retrograde deformation is confined to rare shear bands and tension gashes.

Early attempts to determine the age of HP metamorphism in the Western Series resulted in an ambiguous scatter of data: Hervé *et al.* (1974) obtained K–Ar ages of 329 ± 22 Ma and 211 ± 32 Ma for glaucophane in the Pichilemu blueschists, whereas K–Ar white mica ages in metapelites from the same area were 208 ± 5 Ma (Hervé *et al.*, 1984) and 216 ± 6 Ma (Gana & Hervé, 1983).

In most of the basement of the Coastal Cordillera the Eastern Series rocks comprise very low grade metagreywackes and metapelites without metabasite intercalations. They show stratigraphic continuity at outcrop scale, as well as a non-transposed first folding of bedding planes, and represent a weakly deformed retro-wedge area (Hervé *et al.*, 1988; Willner *et al.*, 2000). In the
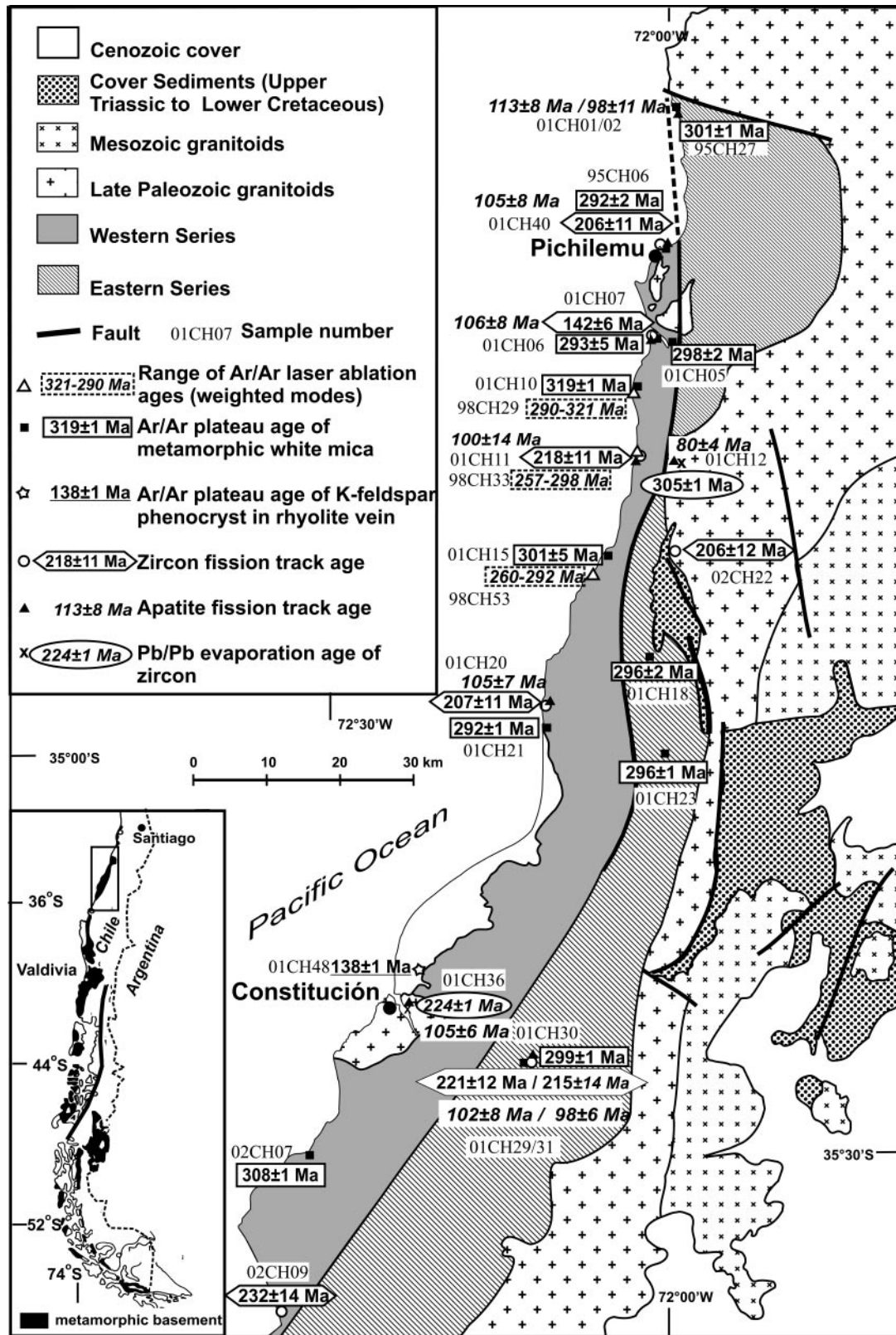
Fig. 1. Geological map with distribution of ages obtained as part of this study.

Table 1: Localities of samples dated in this study

Sample number and location	Latitude	Longitude	Rock type
Eastern Series			
01CH01 Tanumé beach	34°13·49′S	71°58·57′W	Metagreywacke
01CH02 Tanumé beach	34°13·49′S	71°58·57′W	Metagreywacke
95CH27 Tanumé beach	34°13·49′S	71°58·57′W	Andalusite schist
01CH18 Roadcut north of Vichuquén	34°51·56′S	72°03·56′W	Quartz vein
01CH23 Roadcut west of Licantén	34°59·05′S	72°00·05′W	Quartz vein
01CH29 Huinganes station	35°25·10′S	72°19·50′W	Metagreywacke
01CH30 Huinganes station	35°25·10′S	72°19·50′W	Quartz vein
01CH31 Huinganes station	35°25·10′S	72°19·50′W	Metagreywacke
Western Series			
95CH06 Pichilemu—Infiernillo	34°23·55′S	72°01·44′W	Blueschist
01CH40 Pichilemu—La Puntilla	34°22·60′S	72°00·80′W	Metagreywacke
01CH05 El Molino gorge east of Cahuil	34°29·78′S	71°59·83′W	Blueschist
01CH07 Coast south of Laguna Cahuil	34°29·70′S	72°01·45′W	Metagreywacke
01CH06 Coast south of Laguna Cahuil	34°29·70′S	72°01·45′W	Quartz vein
01CH10 Coast south of Punta Sirena	34°32·24′S	72°02·63′W	Garnet mica-schist
98CH29 Coast south of Punta Sirena	34°32·24′S	72°02·63′W	Garnet mica-schist
01CH11 Coast south of Bucalemu	34°38·20′S	72°04·05′W	Metagreywacke
98CH33 Coast south of Bucalemu	34°38·20′S	72°04·05′W	Metagreywacke
01CH15 Coast south of Llico	34°45·29′S	72°05·38′W	Quartz vein
98CH53 Coast south of Llico	34°45·29′S	72°05·38′W	Metagreywacke
01CH21 Coast at Iloca	34°57·30′S	72°13·44′W	Quartz vein
01CH20 Coast at Duao	34°53·13′S	72°10·19′W	Metagreywacke
02CH07 Coast at Los Pellines	35°28·42′S	72°30·17′W	Quartz vein
02CH09 Coast south of Pellahue	35°49·50′S	72°35·00′W	Metagreywacke
Palaeozoic intrusions			
02CH22 Roadcut NE of Vichuquén	34°50·10′S	71°57·01′W	Biotite granite
01CH12 Roadcut at Valdivia	34°40·54′S	72°00·18′W	Biotite granite
01CH36 Constitución, Rio Maule Bridge	35°20·10′S	72°25·50′W	Biotite
01CH48 Roadcut north of Junquillar	35°17·16′S	72°21·50′W	Rhyolite vein
01CH47 Central Rapel power station	34°02·41′S	71°35·22′W	Granodiorite

study area the rocks of the Eastern Series are entirely overprinted by a post-kinematic HT–LP metamorphic event. Mapped north–south-trending metamorphic zones display an increasing metamorphic grade towards the batholith of the late Palaeozoic arc intruding the Eastern Series in its eastern part (González Bonorino, 1971). Peak *PT* conditions range from *c.* 400°C to 720°C at 3 ± 0·5 kbar, indicating a regional metamorphic event causing a thermal dome with the batholith in its core (Willner, 2005).

In contrast to the Western Series, the retrograde overprint in the Eastern Series is rather localized and caused only late very low grade effects. The first HT metamorphic ages in the Eastern Series were determined by Hervé *et al.* (1984), including K–Ar whole-rock ages of 299 ± 10 Ma (schist) and a biotite age of 278 ± 7 Ma. Whole-rock Rb–Sr errorchrons for a schist and a gneiss from the Eastern Series yielded ages of 347 ± 32 Ma and 368 ± 42 Ma (Hervé *et al.*, 1984). Although these data are presumably a mixture of metamorphic and inherited ages, they are markedly older than a similar Rb–Sr errorchron for metabasite and metapelite samples from the Western Series (311 ± 10 Ma), suggesting a younger protolith age for the latter (Hervé *et al.*, 1984).

The boundary between the two basement series is transitional in the south of the study area, with a second flat foliation becoming increasingly penetrative approaching the Western Series. However, in the north this boundary is marked by a late brittle reverse structure, the Pichilemu–Vichuquén Fault (Fig. 1), which cuts major

isograds of the HT metamorphic overpint, requiring at least a few kilometres of vertical offset. Toward the south it dies out.

Palaeozoic calc-alkaline granitoids constitute the main part of the Southern Coastal Batholith of central Chile, which intruded the Eastern Series (Hervé *et al.*, 1988). The batholith appears homogeneous over much of its extent and is composed of tonalitic to granitic portions. Hervé *et al.* (1988) determined Rb–Sr whole-rock isochron ages for three granitoids in the Valparaiso region at 299 ± 31 Ma, 292 ± 2 Ma, and 308 ± 15 Ma (north of the study area), similar to earlier Rb–Sr whole-rock ages of 296 ± 5 and 319 ± 17 Ma (Cordani *et al.*, 1976; Shibata *et al.*, 1984). Two granitoids south of the study area yielded Rb–Sr whole-rock isochron ages of 294 ± 24 Ma and 312 ± 35 Ma (Hervé *et al.*, 1976, 1988) and K–Ar biotite ages from the Southern Coastal Batholith range from 284 ± 5 Ma to 306 ± 6 Ma (Hervé *et al.*, 1988). All ages suggest a narrow age range for the major volume of the late Palaeozoic granitoids in the Southern Coastal Batholith of north–central Chile, consistent with data from south–central Chile (at $\sim 40°$S), where Martin *et al.* (1999) determined U–Pb zircon ages in granites of 282 ± 4 to 306 ± 3 Ma. The granitoids of the Palaeozoic magmatic arc are characterized by relatively high $^{87}Sr/^{86}Sr$ ratios (0·706–0·707), indicating a large component of recycled crustal rocks in their petrogenesis (Hervé *et al.*, 1988). Jurassic and early Cretaceous calc-alkaline intrusions indicate that the Mesozoic magmatic arc essentially remained at the site of the Palaeozoic arc (Hervé *et al.*, 1988).

Small post-tectonic, high-level monzogranitic plutons with K–Ar biotite ages between 215 ± 4 Ma and 202 ± 6 Ma occur within the Western Series (Gana & Hervé, 1983; Hervé *et al.*, 1988). The youngest intrusions in the Western Series are scattered, local, post-tectonic basalt dykes of decimetre to metre thickness as well as rarer rhyolitic dykes. The oldest cover rocks unconformably overlying the Eastern Series and the Southern Coastal Batholith are an Upper Triassic marine siliciclastic sequence with minor volcanic rocks (Carnian–Norian stratigraphic age; Corvalán, 1976; Belmar *et al.*, 2002), grading into a similar sequence of early Jurassic age. Belmar *et al.* (2004) dated diagenesis in shales in the lower part of the sequence at 206 ± 6 Ma, and very low grade burial metamorphic conditions at 181 ± 6 to 184 ± 4 Ma (K–Ar $<2\,\mu m$ illite fraction). Thermometric results point to deposition under a high geothermal gradient of $>35°C/km$ in an extensional geodynamic setting and an intra-arc position (Belmar *et al.*, 2002).

$^{40}Ar/^{39}Ar$ GEOCHRONOLOGY

Two independent approaches were used to obtain ages reflecting peak metamorphic conditions and retrograde overprints from white mica: (1) laser step-heating analysis of single large grains (1·5–2 mm) or aggregates of large grains (0·5–1·0 mm); (2) *in situ* UV laser ablation analysis on single grains (0·2–0·4 mm) or parts of grains in a defined fabric of a polished thick section. We adopt the commonly accepted value of ~ 350–$420°C$ as the white mica Ar closure temperature (McDougall & Harrison, 1999, and references therein). Hence, mineral formation ages should be expected from the Western Series analyses, where peak temperatures were within the above range, whereas cooling ages should be expected from the Eastern Series, where peak temperature ranged between ~ 450 and $720°C$ (Willner, 2005).

Although Ar diffusive loss from a crystal structure is commonly assumed to be dependent on temperature and cooling rate, Villa (1998) argued that strain and fluid availability are more important in isotope redistribution and that many estimates of the closure temperature are too low. This point was originally made by Wijbrans & McDougall (1986), who suggested that closure by volume diffusion will occur only in the absence of other faster processes such as strain-induced recrystallization. Hence, to obtain meaningful ages for the peak of metamorphism, large crystals were separated from small-scale, visibly undeformed volumes that can be regarded as relatively monomineralic. Thus the isotopic system can be assumed to have remained closed, because exchange with different neighbouring phases is minimized, and the relatively low surface/volume ratio also keeps interaction with fluids (diffusion, continuing mineral growth) to a minimum.

Western Series

We separated coarse phengite [Si 3·2–3·37 atoms per formula unit (a.p.f.u.)] from near-monomineralic enrichments at the contacts of quartz veins within the metapsammopelitic rocks of the Western Series (four samples; Fig. 2; Tables 1 and 2), where no contamination with other phases such as chlorite or amphibole is observed. These veins contain minerals that reflect peak metamorphic conditions (phengite, Na–Ca-amphibole, chlorite, epidote) and are oriented parallel to the penetrative second foliation. The selected grains preserved no orientation and were undeformed. Furthermore, two phengite aggregates (Fig. 2, Tables 1 and 2; Si 3·50–3·53 a.p.f.u.) were separated from nearly monomineralic millimetre-sized lamellae in blueschists, which developed parallel to the second foliation and contain coarse unoriented grains. These blueschists are from the only two localities where glaucophane is developed and coexists with phengite, epidote, chlorite, quartz, albite and titanite.

The six white mica samples from the Western Series yielded plateau ages between 292 ± 1 Ma and 308 ± 1 Ma (Fig. 2; Table 2). Ages derived from normal and
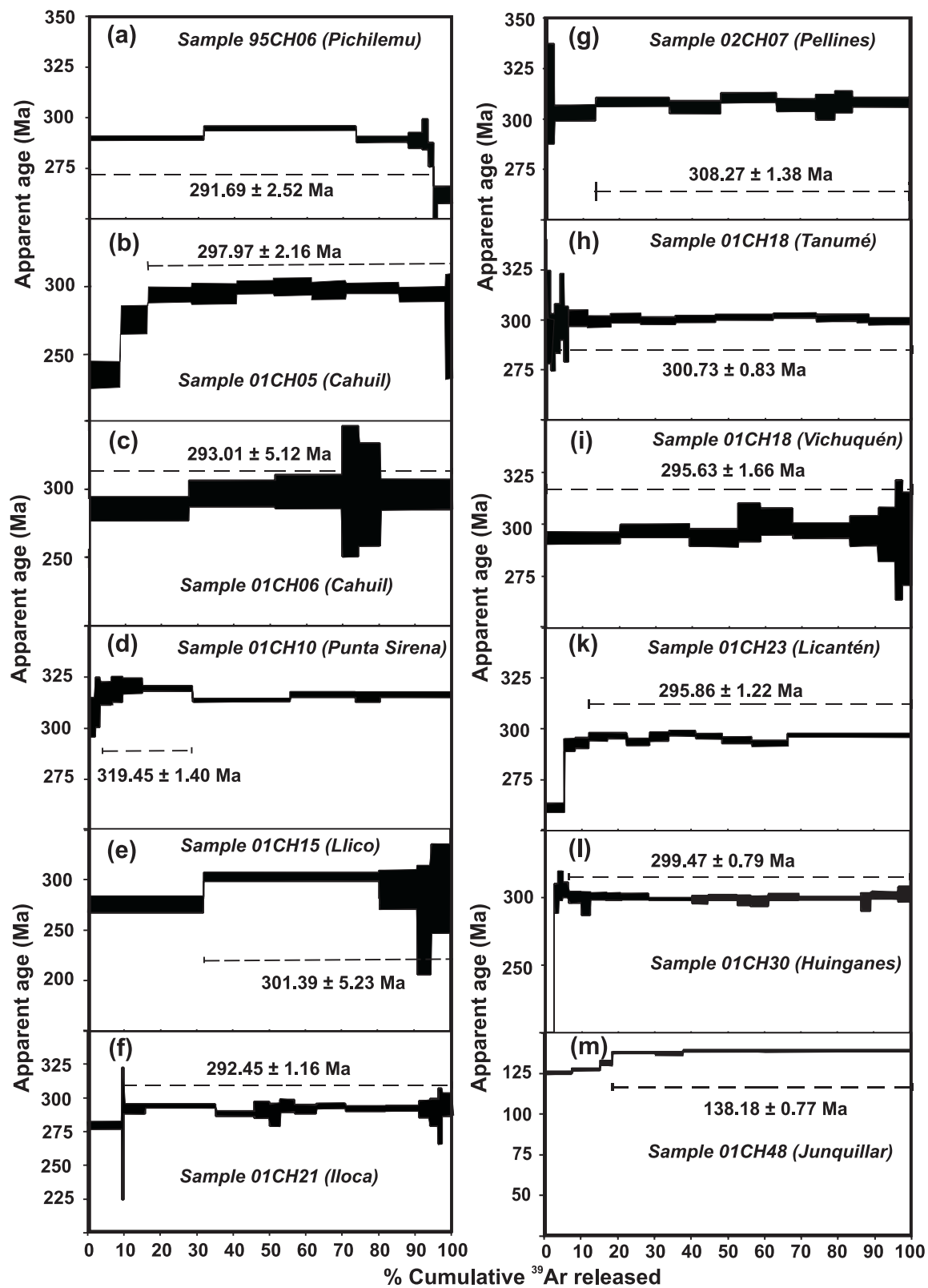
Fig. 2. ^{40}Ar/^{39}Ar release spectra and ages for the basement in central Chile (34°–35°30′S). Western Series: phengite from blueschist (a, b), from quartz veins (c, e–g), and garnet mica-schist (d). Eastern Series: muscovite from quartz veins (h–l). K-feldspar from rhyolite dyke (m). (See Table 2.)

Table 2: $^{40}Ar/^{39}Ar$ step heating ages of white mica from the metamorphic basement (34°–35° 30′S)

Sample	Mineral	Si p.f.u. white mica	Grain type*	Grain size (mm)	Weighted plateau	Total fusion	Normal isochron	Inverse isochron	MSWD	*J* value
Western Series										
95CH06	Phengite	3·50	A	0·5	291·69 ± 2·52	290·23 ± 0·81	295·74 ± 2·71	296·76 ± 2·29	18·04	0·007142
01CH05	Phengite	3·53	A	0·5	297·97 ± 2·16	290·54 ± 2·27	295·47 ± 3·53	291·05 ± 20·10	0·79	0·007145
01CH06	Phengite	3·37	A	0·5–1	293·01 ± 5·12	293·80 ± 5·65	297·89 ± 61·20	302·87 ± 223·7	0·90	0·007145
01CH10	Phengite	3·35	A	0·5	319·45 ± 1·40	216·14 ± 0·86	319·40 ± 1·61	319·57 ± 1·45	0·46	0·007142
01CH15	Phengite	3·20	S	1·5	301·39 ± 5·23	290·11 ± 4·98	305·41 ± 2·42	305·37 ± 2·32	1·46	0·007142
01CH21	Phengite	3·25	A	0·5–1	292·45 ± 1·16	290·78 ± 1·04	293·48 ± 1·17	299·41 ± 4·52	1·95	0·007145
02CH07	Phengite	3·25	S	2	308·27 ± 1·38	307·53 ± 1·30	310·87 ± 1·30	311·99 ± 6·42	1·27	0·007142
01CH48	K-feldspar		S	10	138·27 ± 0·77	136·38 ± 0·44	139·33 ± 5·27	139·42 ± 5·17	4·96	0·007142
Eastern Series										
95CH27	Muscovite	3·04	S	2	300·73 ± 0·83	299·86 ± 0·94	300·84 ± 2·70	300·42 ± 0·85	1·25	0·007148
01CH18	Muscovite	3·18	S	1·5	295·63 ± 1·66	296·03 ± 1·90	297·29 ± 2·26	297·02 ± 2·10	1·00	0·007142
01CH23	Muscovite	3·05	S	0·5–1	295·86 ± 1·22	293·79 ± 0·71	297·12 ± 2·10	295·36 ± 2·74	5·71	0·007142
01CH30	Muscovite	3·18	A	0·5–1	299·47 ± 0·79	297·48 ± 0·77	300·42 ± 0·77	297·73 ± 2·34	0·99	0·007145

*A, aggregate of grains; S, single grain.
Mineral samples were irradiated for 24 h using the d-lined RODEO facility of HFR Petten. Correction factors for interferences of Ca and K isotopes were 0·000699 for $^{39}Ar/^{37}Ar$, 0·000270 for $^{36}Ar/^{37}Ar$, and 0·00183 for $^{40}Ar/^{39}Ar$. In-house standard sanidine DRA (age 25·26 ± 0·07 Ma, Wijbrans *et al.*, 1995) was used as a flux monitor during irradiation. The step-heating experiments were carried out with the VULKAAN laser-probe facility at Vrije Universiteit Amsterdam (Wijbrans *et al.*, 1995). The isotopic composition of the argon gas was measured using a double-focused noble-gas mass spectrometer (MAP 215-50) in static mode. Beam intensities were measured on a secondary electron multiplier detector and switchable pre-amplifier resistor settings (10, 100 and 1000 MOhm) by peak jumping at half mass intervals down from mass 40 to 35·5. The laser power was increased from 0·2–1·1 W to melting over 6–18 steps, with a continuous laser beam (argon ion laser in multi-line mode) defocused to ∼1 mm spot. System blanks were analysed after every four sample extractions. Two samples were analysed in duplicate. All data are presented with a 2σ analytical error. Individual age steps do not include the uncertainty in the *J* value (estimated at 0·3%), which was, however, included in the calculated total gas and plateau ages and errors. Data from each heating step are included as supplementary data on the *Journal of Petrology* website at http://www.petrology.oupjournals.org.

inverse isochrons ($^{40}Ar/^{36}Ar$ vs $^{39}Ar/^{36}Ar$ and $^{36}Ar/^{40}Ar$ vs $^{39}Ar/^{40}Ar$ plots, respectively) are within error of the plateau ages. Although excess argon is frequently reported from HP–LT areas (De Jong *et al.*, 2001), no indication about a potential excess argon component is detectable in the isochron plots of any of the samples. We exclude the possibility of this effect for our samples for the following reasons: (1) Rb–Sr dating of phengite in blueschists in south–central Chile yielded an identical age to previous $^{40}Ar/^{39}Ar$ dating (Willner *et al.*, 2004); (2) the dated phengite grains from the quartz veins were not in contact with other phases and had the lowest Si contents; (3) incorporation of excess argon in phengite would result in a high scatter of ages, even within a small sampling distance (De Jong *et al.*, 2001), which is not observed for our samples.

We interpret the $^{40}Ar/^{39}Ar$ phengite plateau ages in the Western Series as mineral formation ages reflecting the peak of high-pressure metamorphism. Any influence of deformation can be excluded, because the analysed grains were taken from strain-free domains. In our degassing experiments there was usually a portion of 10–30% of cumulative ^{39}Ar released that contains components that are 10–50 Myr younger. These can be interpreted as late formation ages in agreement with the petrological interpretation of the Western Series, where mineral growth continued during retrograde pressure release (Willner, 2005). A decrease of the Si content is usually observed toward the rims of the phengite grains. Radiogenic ^{40}Ar loss by diffusion during cooling may be an alternative interpretation, but appears improbable, because such effects should be stronger in the white mica of the Eastern Series HT rocks, which yielded age spectra with only minor young low-temperature components (see below).

Phengite from blueschists and from metapsammopelitic rocks reflects the same age range, although Si contents in the metapsammopelitic rocks are considerably lower than in the blueschists. Furthermore, plateau ages for phengite from a blueschist and a metapsammopelite

sample in close proximity are comparable within error (samples 01CH05 and 01CH06), demonstrating that peak metamorphic conditions were attained at the same time within different rock types. A further phengite aggregate was separated from a coarse-grained garnet mica-schist (01CH10). This rare local rock type with the assemblage garnet–chlorite–phengite–quartz–albite–epidote, records the highest PT conditions ($\sim$10–13 kbar, 390–440°C; Willner, 2005). The phengite (Si 3·35 a.p.f.u.) yielded the oldest $^{40}Ar/^{39}Ar$ phengite age of 320 $\pm$ 1 Ma. However, this stage already represents a retrograde stage after isobaric cooling from an earlier higher temperature garnet-forming stage (Willner, 2005). Such characteristics—the highest PT conditions in the study area, isobaric cooling at depth and the age of a retrograde overprint as the oldest age recorded—appear to be typical of rocks formed at the beginning of the accretion process (Willner *et al.*, 2004, and references therein).

There is no detectable regional trend of $^{40}Ar/^{39}Ar$ phengite ages in the investigated area (Fig. 1). Similarly, no clear regional trend was detected for the distribution of maximum burial depths (Willner, 2005). The difference of 30 Myr between the youngest and oldest plateau ages may be explained by the temporal variation of the HP imprint during continuous accretion.

In the Western Series we also aimed to establish age variations within samples and to test the influence of the early penetrative deformation and retrograde mineral growth and recrystallization on the formation of white mica ages younger than the peak metamorphic event. For this purpose, $^{40}Ar/^{39}Ar$ *in situ* UV laser ablation studies were undertaken to date grains at the flanks and hinges of microfolds, several millimetres in size, that were related to the penetrative S_2 foliation. We selected three deformed samples (two metapsammopelitic schists and one garnet mica-schist) characterized by a penetrative crenulation foliation, chemically zoned white mica and recrystallization in the microfold hinges. All analysed white mica grains had variable maximum Si contents (3·21–3·38 a.p.f.u.; Table 3). The mean size of the ablated white mica grains was 50 μm $\times$ 100 μm.

The *in situ* $^{40}Ar/^{39}Ar$ UV laser ablation studies yielded a considerable range of ages in the three selected samples, with a variation of 32–44 Myr between the modes of the oldest and youngest ages (Fig. 3). Absolute age ranges are 259 $\pm$ 1 to 292 $\pm$ 3 Ma, 257 $\pm$ 3 to 301 $\pm$ 2 Ma and 290 $\pm$ 3 to 329 $\pm$ 5 Ma. In the cumulative probability plots (Fig. 3) the respective ranges of the weighted age modes are 260–292 Ma, 257–298 Ma and 290–321 Ma. In each case the oldest age population is within error of the $^{40}Ar/^{39}Ar$ white mica plateau ages obtained from the laser step-heating experiments. The garnet mica-schist again yields the oldest ages. The older ages tend to be concentrated in the cores of the grains, but there is no correlation of age with Si content (Table 3). There is a

tendency to older $^{40}Ar/^{39}Ar$ ages on the flanks of microfolds in samples 98CH29 and 98CH53, but older ages in the hinges in sample 98CH33 (Fig. 3). This is also evident in the weighted mean ages, whereas the errors of the unweighted mean ages largely overlap. Hence there is no discernible effect of deformation on the age distribution. We suggest that the conspicuous retrograde mineral growth and recrystallization during decompression under excess water conditions produced the detected age variation. However, continuous deformation during the last stages of the penetrative D_2 deformation, resulting in reopening of the K–Ar system during retrograde reaction, cannot be excluded. Based on the above interpretation, the youngest ages reflect the time when observable retrograde mineral growth ended in each sample slightly above 300°C (Willner, 2005). Grain size evidently has an important influence on the preservation of the $^{40}Ar/^{39}Ar$ white mica ages during the peak of metamorphism, because the proportion of the late grown material is relatively large in small grains and relatively small in large grains.

Eastern Series

To date peak HT metamorphic conditions in the Eastern Series, muscovite aggregates (Si 3·04–3·18 a.p.f.u.) were separated from three quartz veins similar to those of the Western Series, and also from coarse-grained white mica concentrations near andalusite crystals of 5–10 cm size in a metapelite (Fig. 2; Tables 1 and 2). Whereas the latter grew in areas of major fluid access during HT metamorphism, the other samples occur within metapsammopelites, which were overprinted by a LP–HT event with pervasive new crystallization of biotite and complete recrystallization of white mica (Willner, 2005).

The four muscovite aggregates from the Eastern Series reflect a remarkably narrow age range from 296 $\pm$ 2 to 301 $\pm$ 1 Ma over the *c.* 120 km length of the investigated belt (Fig. 2, Table 2). Younger age components are minor compared with the micas of the Western Series ($<$5% of ^{39}Ar released). In the Eastern Series, deformation after the peak of the HT metamorphism is rare and localized as are retrograde overprints. We interpret these $^{40}Ar/^{39}Ar$ ages as cooling ages, because all rocks were heated well above the Ar closure temperature, and were entirely recrystallized and re-equilibrated (Willner, 2005). Coarse muscovites from sample 95CH27 are intergrown with large porphyroblasts of andalusite that formed during the HT imprint. The uniform cooling ages should be close to the age for the peak of HT/LP metamorphism considering that the HT metamorphism represents an extended thermal dome related to the Palaeozoic batholith cooling to temperatures around 350°C prevailing at the same time in the Western Series. The limited low-temperature younger age components also preclude long-term cooling.

Table 3: $^{40}Ar/^{39}Ar$ *isotopic ratios and ages of single white mica grains measured by UV laser ablation (Western Series)*

Grain	Position	Si (a.p.f.u.)	Age (Ma)	±	$^{40}Ar*/^{39}Ar$	±	$^{40}Ar/^{39}Ar$	±	$^{38}Ar/^{39}Ar$	±	$^{37}Ar/^{39}Ar$	±	$^{36}Ar/^{39}Ar$	±	^{39}Ar (cm^3)
Sample 98CH29															
P13	HingeR	3·19	290·26	2·55	37·97	0·31	40·18	0·19	0·01200	0·00004	0·02362	0·01549	0·00746	0·00083	1·63E − 12
P13	HingeC	n.d.	316·01	2·06	41·65	0·21	42·53	0·11	0·00996	0·00001	0·07441	0·01259	0·00300	0·00060	2·25E − 12
P3	HingeR	3·18	304·23	2·45	39·96	0·29	40·59	0·26	0·01199	0·00043	0·02282	0·00612	0·00215	0·00043	3·15E − 12
P11	HingeR	3·18	305·88	1·55	40·19	0·09	40·82	0·06	0·01156	0·00053	0·04637	0·00556	0·00213	0·00024	5·69E − 12
P11	HingeC	3·23	306·48	1·48	40·28	0·06	40·89	0·03	0·01152	0·00019	0·02427	0·00442	0·00207	0·00019	7·16E − 12
P5	Hinge	3·21	307·93	8·25	40·49	1·16	42·78	0·18	0·01607	0·00006	0·05528	0·04054	0·00777	0·00389	6·96E − 13
P15	HingeR	n.d.	309·03	2·38	40·64	0·27	41·01	0·24	0·01262	0·00042	0·06714	0·00601	0·00125	0·00042	3·21E − 12
P14	HingeR	n.d.	322·14	1·82	42·53	0·15	43·14	0·14	0·01215	0·00023	0·01892	0·00329	0·00207	0·00023	5·87E − 12
P2	Flank	3·26	309·69	5·74	40·74	0·80	43·01	0·23	0·01338	0·00259	0·34395	0·03423	0·00769	0·00259	5·23E − 13
P16	FlankC	n.d.	314·55	1·60	41·43	0·10	41·89	0·06	0·01253	0·00013	0·01728	0·00384	0·00153	0·00026	1·06E − 11
P9	FlankC	3·30	320·49	1·62	42·29	0·10	42·89	0·08	0·01291	0·00019	0·02574	0·00437	0·00205	0·00019	7·26E − 12
P10	Flank	3·26	328·81	4·88	43·49	0·67	43·49	0·20	0·01119	0·00217	0·24646	0·02860	0·00000	0·00000	6·25E − 13
Sample 98CH33															
P5	Flank	3·20	257·07	3·21	33·30	0·41	36·08	0·12	0·01393	0·00004	0·12688	0·01962	0·00941	0·00135	1·00E − 12
P6	Flank	3·17	257·44	5·82	33·35	0·79	36·15	0·38	0·01231	0·00009	0·19918	0·00142	0·00948	0·00238	1·14E − 12
P11	Flank	3·24	276·84	2·51	36·06	0·30	36·93	0·09	0·01725	0·00098	0·05145	0·01012	0·00294	0·00098	1·38E − 12
P12	Flank	3·19	297·80	1·55	39·02	0·10	39·12	0·03	0·01260	0·00033	0·00690	0·00480	0·00033	0·00033	4·11E − 12
P4	Hinge	3·27	279·43	2·58	36·43	0·31	38·54	0·09	0·01266	0·00003	0·05343	0·01052	0·00714	0·00102	1·33E − 12
P9	Hinge	3·20	287·01	4·81	37·50	0·65	38·70	0·25	0·01056	0·00002	0·05340	0·01051	0·00408	0·00205	1·32E − 12
P13	Hinge	3·22	292·97	1·73	38·34	0·15	38·86	0·11	0·01575	0·00035	0·00000	0·00366	0·00177	0·00035	3·82E − 12
P14	Hinge	3·21	301·50	1·63	39·55	0·12	41·77	0·04	0·01264	0·00040	0·01242	0·00408	0·00750	0·00039	3·43E − 12
Sample 98CH53															
P1	Hinge	3·14	259·48	1·47	33·59	0·12	35·95	0·12	0·00826	0·00002	0·07692	0·01514	0·00798	0·00002	1·36E − 12
P12	Hinge	3·12	262·56	4·57	34·02	0·61	35·43	0·05	0·01709	0·00001	0·14166	0·02091	0·00479	0·00207	1·97E − 12
P13	Hinge	3·09	268·05	9·51	34·78	1·32	37·36	0·19	0·01824	0·00008	0·40874	0·08939	0·00873	0·00441	6·14E − 13
P2	Hinge	3·12	268·74	7·24	34·88	1·00	35·71	0·53	0·01372	0·00003	0·16046	0·01725	0·00281	0·00285	1·43E − 12
P10	Flank	3·11	271·23	1·38	35·23	0·08	37·17	0·08	0·01224	0·00002	0·05746	0·00998	0·00657	0·00001	2·06E − 12
P6	Flank	3·14	271·43	4·84	35·26	0·65	37·27	0·35	0·01415	0·00002	0·09890	0·01132	0·00682	0·00187	2·18E − 12
P8	Flank	3·18	271·85	5·52	35·32	0·75	36·55	0·08	0·01219	0·00002	0·09531	0·02558	0·00419	0·00253	1·61E − 12
P9	Flank	3·18	291·77	3·29	38·12	0·42	38·12	0·11	0·01288	0·00004	0·06417	0·02806	0·00000	0·00000	1·96E − 12

n.d., not determined; C, core; R, rim. Two polished sections (10 mm × 10 mm × 150 μm) were prepared for each sample. Biotite age standard Tinto B (K–Ar age of 409·24 ± 0·71 Ma) was loaded as a flux monitor at 5 mm intervals along the Al irradiation package, which was irradiated at the McMaster University Nuclear Reactor in Hamilton, Ontario, for 20h. A New Wave Research LUV 213X 4 mJ pulsed quintupled Nd–YAG laser ($\lambda = 213$ nm) was used for ablation at the Western Australian Argon Isotope Facility in Perth. Gases released by laser ablation analysis were 'gettered' using three SAES AP10 getter pumps to remove all active gases. Remaining noble gases were equilibrated into a high-sensitivity MAP 215-50 mass spectrometer, operated at a resolution of 600, and fitted with a Balzers SEV 217 multiplier. The mean 5 min extraction system blank Ar isotope measurements obtained during the experiments were $8·9 \times 10^{-12}$, $5·4 \times 10^{-15}$, $8·1 \times 10^{-15}$, $1·2 \times 10^{-13}$ and $4·9 \times 10^{-14}$ cm^3 STP for ^{40}Ar, ^{39}Ar, ^{38}Ar, ^{37}Ar, ^{36}Ar, respectively. The Ca and K correction factors used in the data reduction were $^{39}Ar/^{37}Ar_{Ca} = 0·00065$, $^{36}Ar/^{37}Ar_{Ca} = 0·000255$ and $^{40}Ar/^{36}Ar_{K} = 0·0015$. The decay constant used is that of Steiger & Jäger (1977). J values used for samples were 0·004597 for 98CH29, 0·004599 for 98CH33, and 0·004605 for 98CH53. Errors are 1σ.
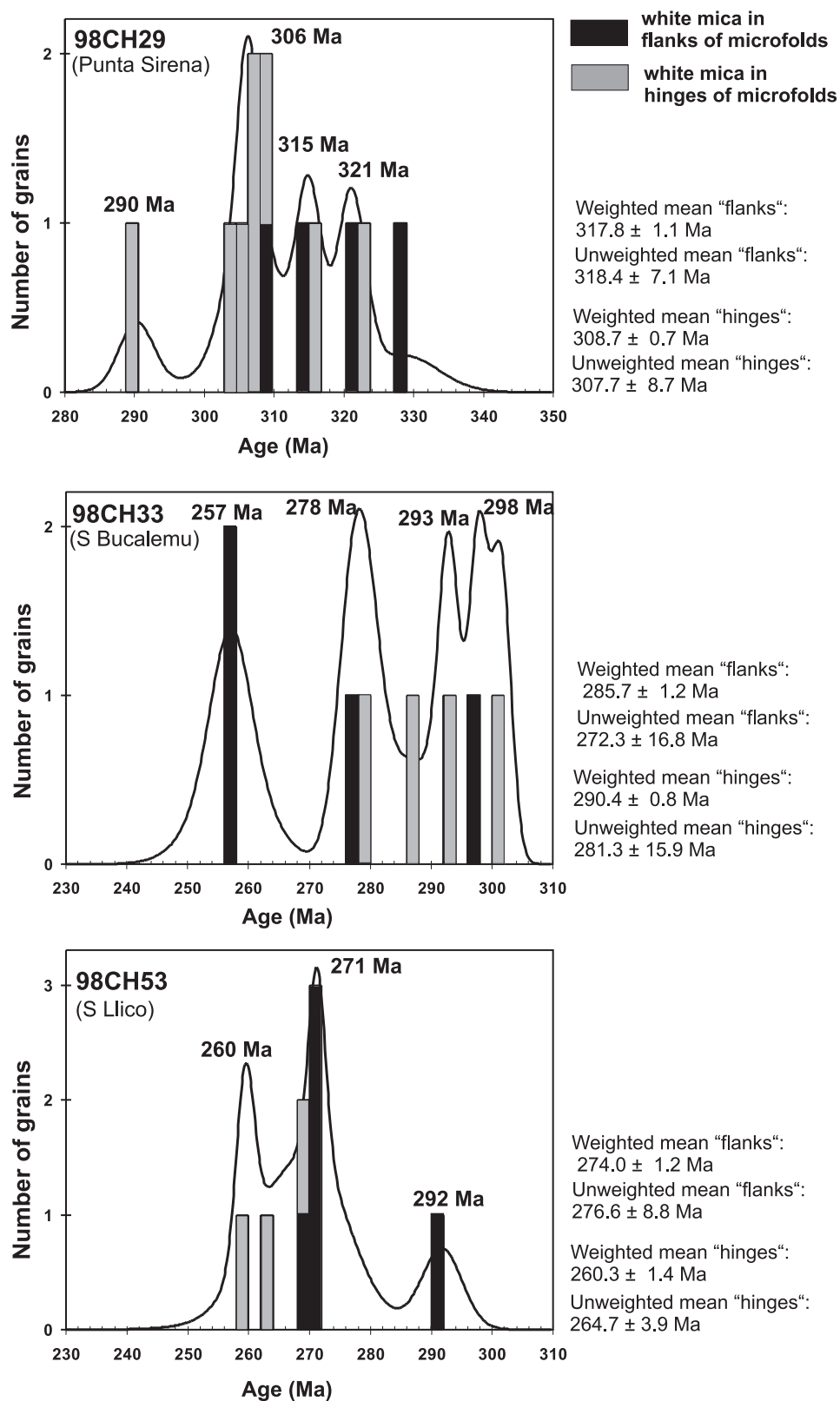
Fig. 3. Histograms and cumulative probability plots for $^{40}Ar/^{39}Ar$ single grain laser ablation ages of white micas from metapsammopelitic schists of the Western Series in central Chile (34°–35°30′S). (See Table 3.)

Rhyolite dykes

Rhyolite sample 01CH47 represents part of a post-tectonic and post-metamorphic bimodal intrusive suite of unknown age, occasionally found as 0·1–1 m rhyolitic and basaltic dykes within the basement. Fragments (1–3 mm) of 0·5–1 cm euhedral crystals of K-feldspar were separated from a rhyolite for $^{40}Ar/^{39}Ar$ laser step-heating. X-ray diffraction analysis indicates that the K-feldspar is microcline. The $^{40}Ar/^{39}Ar$ laser step-heating analyses yielded a well-defined $^{40}Ar/^{39}Ar$ plateau age of 138 ± 1 Ma, with ~20% of released, low-temperature, cumulative ^{39}Ar reflecting younger age information down to 125 Ma. The closure temperature for potassic feldspar appears to be variable (125–350°C) and crystal domain-size dependent (Harrison *et al.*, 1991). Nevertheless, the age range broadly corresponds to the temperature that may be inferred for the surrounding rocks at that stage. In spite of the strong overprint caused by hydrothermal alteration, which mainly affects the plagioclase phenocrysts, we interpret the microcline plateau age as a cooling age close to the crystallization age of the rhyolite, and the younger age portion as a result of prolonged cooling in accordance with slow cooling of the surrounding basement rocks.

FISSION-TRACK GEOCHRONOLOGY
Zircon fission-track data

To obtain time markers along the cooling and exhumation paths of both metamorphic series, fission-track (FT) dating of zircon and apatite was undertaken. For zircon FT dating five metagreywacke samples were selected from the Western Series, one metagreywacke sample from the Eastern Series and one granite sample (Fig. 4; Tables 1 and 4). For pristine zircon, annealing of fission tracks over geological time begins at ~250 ± 20°C, with total resetting occurring above ~310–350°C (Tagami *et al.*, 1998; Brix *et al.*, 2002). Each individual FT age was determined by calculating a central age (Galbraith & Laslett, 1993) from up to 20 individual grain ages from each sample. The single grain FT age data are described by their age dispersion and graphically presented by radial plots (Galbraith, 1990; Figs 4 and 5).

Because the upper temperature limit of zircon partial annealing was exceeded in all rocks from the study area, FT ages are expected to represent cooling ages. Given mean cooling rates of around 1°C/Myr during exhumation, as shown below, we preferred to use a closure temperature of 270–280°C (Rahn *et al.*, 2004) for our study.

With one exception, zircon FT ages range from 206 ± 11 Ma to 221 ± 12 Ma with no geographical trend within the study area (Figs 1 and 4). There is no difference between the ages of the Western and Eastern Series, implying that both belts uniformly cooled through the 280°C isotherm a considerable time after reaching peak metamorphic conditions. One sample, however, is exceptional in yielding an age of 142 ± 7 Ma (sample 01CH07). This is identical, within error, to the Ar/Ar plateau age for the rhyolite dyke from Junquillar at 138 ± 1 Ma (sample 01CH47). The age similarity suggests that this reflects a localized resetting during a Jurassic magmatic event. At Punta Lobos, 5 km to the north of the 01CH07 sample locality, a subhorizontal gabbroic sill of 5 m thickness is exposed at the surface, which might belong to the same bimodal Jurassic magmatic suite.

Fission-track data of apatite

Grains were separated from four metagreywacke samples from the Western Series, four metagreywacke samples from the Eastern Series and three samples from late Palaeozoic granites (Fig. 5; Tables 1 and 4) for FT dating of apatite. Experimental and borehole data for apatite (e.g. Green *et al.*, 1989; Ketcham *et al.*, 1999) show that fission tracks begin to anneal at a measurable rate above ~60°C, with complete annealing and total resetting of the apatite FT age occurring at 100–120°C. We use 110°C as the mean closure temperature for FT annealing in apatite for our samples. A duplicate FT analysis was made for zircon from sample 01CH31, and two duplicate analyses for apatite from separate samples from the same localities (01CH01/01CH02, 01CH29/01CH31). The resulting ages are comparable within errors in all cases (Figs 4 and 5).

Apatite FT ages predominantly range from 98 ± 6 Ma to 113 ± 8 Ma without displaying any clear regional trend or difference between the two series (Figs 1 and 5). All apatite FT ages are regarded as cooling ages. One apatite FT age of 80 ± 4 Ma from the granite batholith directly east of the Pichilemu–Vichuquén Fault suggests a genetic relationship with the late activity along this fault.

The relatively long apatite track lengths with unimodal, slightly negatively skewed distributions imply relatively fast mid-Cretaceous cooling rates across the partial annealing zone. A subsequent slowdown in cooling rate is implied by the fact that the samples have remained below ~60°C since about 95 Ma. The latter constraint limits post-mid-Cretaceous cooling rates to ≤1°C/Myr, equivalent to exhumation rates of <0·03–0·04 mm/yr assuming a geothermal gradient of 30°C/km.

We also modelled the time–temperature history from apatite FT data using the MonteTrax software (Gallagher, 1995) and the apatite FT annealing model of Laslett *et al.* (1987). The results are illustrated in Fig. 6 for representative samples from the Western Series, Eastern Series and a Late Palaeozoic granitoid respectively. Because the apatite FT data cannot be used to constrain
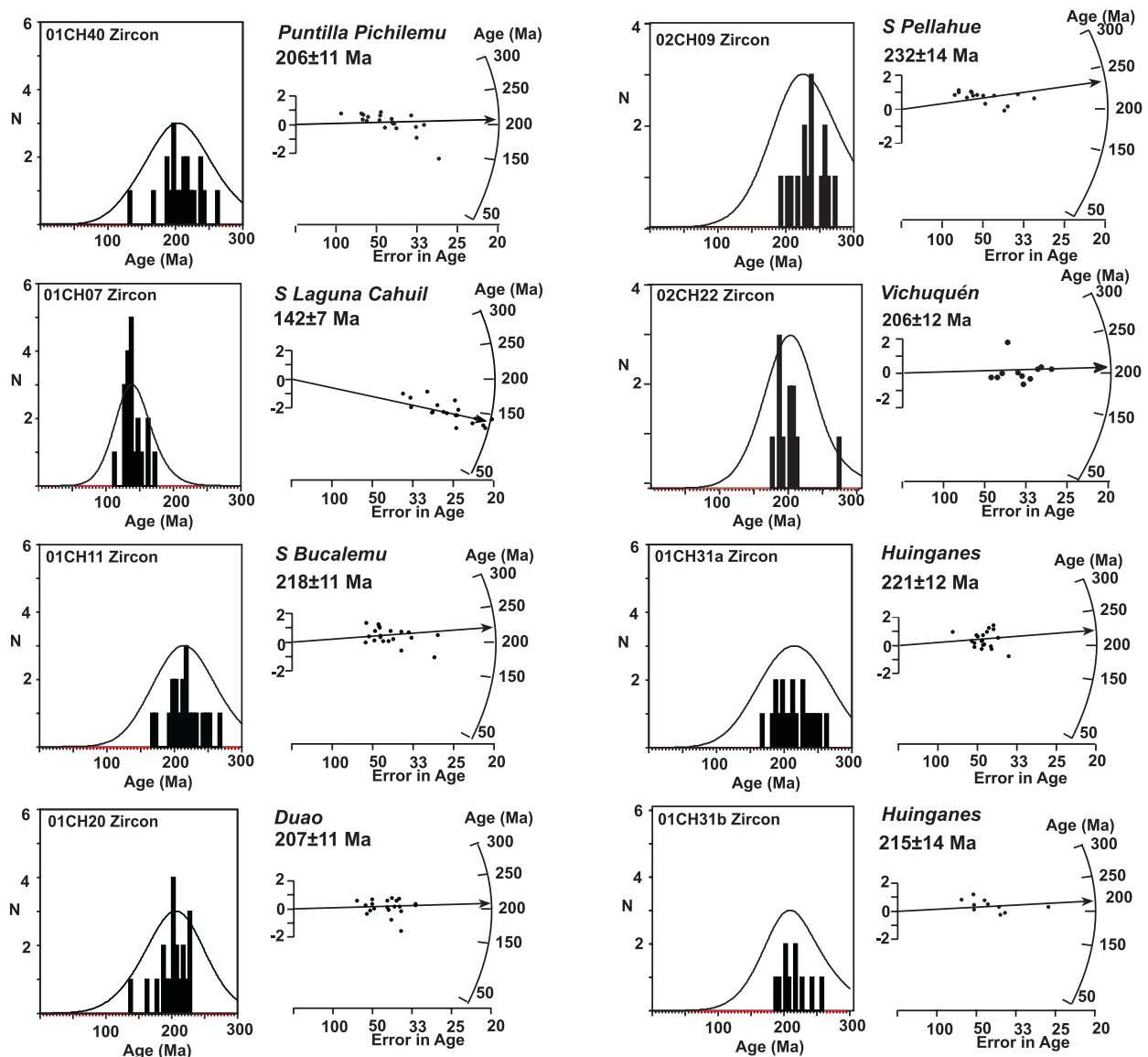
Fig. 4. Histogram and radial plot representation of the zircon single grain fission-track age data from basement rocks of central Chile (34°–35°30′S). (See Table 4.) In the radial plots, x-scale is $1/\sigma$, y-scale is $(z - z_0)/\sigma$, and z-scale represents the age.

the pre-mid-Cretaceous thermal history, two alternative pre-mid-Cretaceous scenarios were modelled: (1) continuous slow cooling from 230°C at 210 Ma to temperatures of $\leq$130°C between 120 and 80 Ma; (2) rapid cooling from 230°C at 210 Ma to surface conditions (10°C) at 200 Ma, followed by slow reburial-related heating to temperatures of $\geq$110°C between 120 and 80 Ma. The second scenario is based on the presence of unconformably overlying Upper Triassic sedimentary rocks. The modelled samples and both scenarios require rapid cooling of all basement rocks through the apatite FT partial annealing zone between about 115 Ma and 90 Ma, followed by a slowdown in cooling rates until present exposure of the sampled rocks at the surface. Cooling rates of at least 3–5°C/Myr during mid-Cretaceous times are required to produce the observed apatite FT data. This is almost an order of magnitude higher than the cooling rates required between $\sim$90 Ma and the present in both models ($\sim$0·5°C/Myr), and the cooling rate of 1–2·5°C/Myr at $\sim$210 $-$120 Ma for the post-accretion continuous slow cooling required by scenario (1).

^{207}Pb/^{206}Pb ZIRCON EVAPORATION

Zircons were separated from granite samples to derive time markers for the evolution of the magmatic arc

Table 4: Fission-track data for zircon and apatite from the metamorphic basement between Pichilemu and Constitución (34°–35°30′S)

Sample	N	Track density ($\times 10^6$ tracks/cm^2)			Age dispersion ($P\chi^2$)	Central age (Ma) ($\pm 1\sigma$)	Apatite mean track length (μm $\pm$ 1σ) (N)	SD (μm)
		P_s (N_s)	P_i (N_i)	P_d (N_d)				
Zircon FT data								
01CH07	20	12·42 (4441)	2·223 (795)	0·3928 (5424)	<0·01% (99·9%)	141·8 ± 6·5		
01CH11	20	10·91 (5619)	1·264 (651)	0·3932 (5430)	<0·01% (99·1%)	218·1 ± 10·6		
01CH20	20	13·11 (4599)	1·601 (562)	0·3937 (5437)	<0·01% (99·9%)	207·2 ± 10·6		
01CH31a	20	16·21 (4500)	1·855 (515)	0·3942 (5443)	<0·01% (99·6%)	221·3 ± 11·7		
01CH31b	10	15·53 (2659)	1·828 (313)	0·3946 (5450)	<0·01% (98·5%)	215·4 ± 14·0		
01CH40	20	13·00 (4220)	1·602 (520)	0·3951 (5456)	<0·01% (97·2%)	206·2 ± 10·9		
02CH09	15	12·17 (3413)	1·430 (401)	0·4242 (5858)	<0·01% (99·9%)	231·7 ± 13·5		
02CH22	11	15·28 (3377)	2·018 (448)	0·4232 (5844)	0·04% (87·8%)	206·1 ± 11·6		
Apatite FT data								
01CH01	20	2·028 (406)	3·835 (768)	1·197 (8266)	0·12% (86·4%)	112·5 ± 8·1	13·66 ± 0·12 (100)	1·24
01CH02	14	0·813 (128)	1·766 (278)	1·195 (8250)	<0·01% (99·9%)	98·0 ± 11·1	13·86 ± 0·18 (41)	1·16
01CH07	20	1·290 (376)	2·594 (756)	1·192 (8233)	<0·01% (99·8%)	105·5 ± 7·7	14·02 ± 0·12 (100)	1·24
01CH11	6	0·385 (85)	0·819 (181)	1·190 (8216)	<0·01% (89·2%)	99·5 ± 13·6	14·00 ± 0·19 (3)	0·26
01CH12	20	2·026 (929)	5·333 (2446)	1·187 (8199)	0·20% (75·0%)	80·4 ± 4·3	12·93 ± 0·19 (100)	1·88
01CH20	16	1·451 (577)	2·922 (1162)	1·183 (8165)	0·05% (90·0%)	104·5 ± 6·6	13·53 ± 0·18 (64)	1·43
01CH29	20	1·159 (325)	2·386 (669)	1·178 (8132)	<0·01% (99·8%)	101·9 ± 7·9	12·84 ± 0·15 (100)	1·49
01CH31	20	1·221 (560)	2·611 (1197)	1·175 (8115)	0·08% (93·3%)	97·9 ± 6·2	12·73 ± 0·19 (100)	1·87
01CH36	20	3·529 (1189)	7·081 (2386)	1·173 (8098)	6·54% (21·4%)	104·6 ± 5·6	14·10 ± 0·12 (100)	1·17
01CH40	16	1·582 (402)	3·137 (797)	1·170 (8081)	<0·01% (98·9%)	105·0 ± 7·5	13·60 ± 0·21 (63)	1·63
01CH47	20	1·264 (658)	2·712 (1412)	1·168 (8065)	<0·01% (98·4%)	96·9 ± 5·8	14·33 ± 0·09 (100)	0·91

For fission-track analysis, mounting, polishing and etching of zircon and apatite fractions were carried out at Ruhr-Universität Bochum according to Hurford *et al.* (1991). The samples were analysed by the external detector method (using 0·5 for the $4\pi/2\pi$ geometry correction factor) and irradiated with Corning dosimeter glasses (CN2 for zircon and CN5 for apatite) at the Oregon State University Triga Reactor, Corvallis, USA. Central ages (Galbraith & Laslett, 1993) quoted with 1σ errors, were calculated using the IUGS approved zeta-calibration approach of Hurford & Green (1983). Zeta calibration factors of 130·7 ± 2·8 for CN2 (zircon) and 358·8 ± 12·7 for CN5 (apatite) were obtained by repeated calibration against a number of internationally agreed age standards according to Hurford (1990). P_s, spontaneous track density; N_s, number of spontaneous tracks counted; P_i, induced track density in external detector (muscovite); N_i, number of induced tracks counted; P_d, induced track density in external detector adjacent to dosimeter glass; N_d, number of tracks counted to determine P_d; $P\chi^2$, probability of obtaining a χ^2 value for v degrees of freedom where $v = N - 1$ (N is the number of crystals).

relative to the exhumation history of the basement (Figs 1 and 7; Tables 1 and 5). Sample 01CH12 is a biotite granite of intermediate grain size (0·2–0·5 mm), typical of the bulk of the arc batholith. Perthitic microcline, plagioclase and quartz occur in equal amounts. Muscovite and biotite are present as magmatic phases and muscovite as a subsolidus phase grown at the expense of plagioclase. The quantity of extracted euhedral zircon is low. Back-scattered electron images reveal perfect magmatic zonation, but alteration to a hydrous zircon phase along cracks and specific growth zones is common. Two grains contain xenocrystic cores, implying an older crustal component in the magma, as does the presence

of magmatic muscovite. The intrusion level of this granite corresponds to a pressure of ~3·5 kbar or 12 km (Willner, 2005). Because of the small quantity of the recovered grains and their frequent alteration, only one grain fraction of four small grains (*c.* 40–80 μm) could be analysed, yielding a mean ^{207}Pb/^{206}Pb age of 305 ± 3 Ma. This age is interpreted to reflect the time of intrusion and is within the main range of intrusion ages for the late Palaeozoic arc in central Chile between 292 ± 2 and 319 ± 17 Ma (Hervé *et al.* 1988). The age is only slightly older than the HT metamorphism in the Eastern Series, suggesting a relationship between intrusion and HT metamorphism.

Sample 01CH48 was collected about 30 km north of the study area at the power station along the dam of Embalse Rapel. Previous dating (242 ± 10 Ma; K–Ar on biotite; Dávila *et al.* 1979) indicated that this rock may be younger than the bulk of the arc batholith. It is a dark I-type granodiorite of intermediate grain size, composed of plagioclase, quartz and microcline as well as biotite and hornblende in about equal amounts. Accessory titanite, apatite, zircon and magnetite also occur. Zircon is unaltered, euhedral, long-prismatic and displays perfect oscillatory zoning with some resorption of early-formed cores. Four small fractions of 3–4 grains each (*c.* 40–80 μm) were analysed and provided identical $^{207}Pb/^{206}Pb$ ratios that combine to yield a mean age of 257 ± 1 Ma. This shows that calc-alkaline magmatism in the arc continued into Permian times. A single large grain (∼200 μm) produced distinctly higher $^{207}Pb/^{206}Pb$ ratios corresponding to a mean age of 300 ± 3 Ma. We tentatively interpret this age as reflecting crystallization during the main pulse of magmatism in the late Palaeozoic arc.

Subsequently this zircon may have been incorporated as a xenocryst into the younger magma.

Sample 01CH36 is a biotite granite of intermediate grain size, representative of the Constitución pluton that intruded the Western Series during a late stage of its exhumation and thereby produced a contact metamorphic halo of about 100 m width (Godoy, 1970). All zircons are euhedral and long-prismatic with well-developed internal magmatic zoning, but alteration to a hydrous zircon phase in specific growth zones near the rims is common. Four fractions of 3–4 small zircon grains (*c.* 40–80 μm) yielded a mean age of 224 ± 1 Ma. This is interpreted as approximating the time of magma emplacement, setting a time limit for the end of accretion at this locality. The rock evidently belongs to a series of small granite bodies of presumed late Triassic age (Hervé *et al.*, 1988) that intruded into the Western Series. Similarly, an age of 220 ± 5 Ma (Rb/Sr mineral isochron) was derived by Lucassen *et al.* (2004) for a granite within the Western Series in south–central Chile.
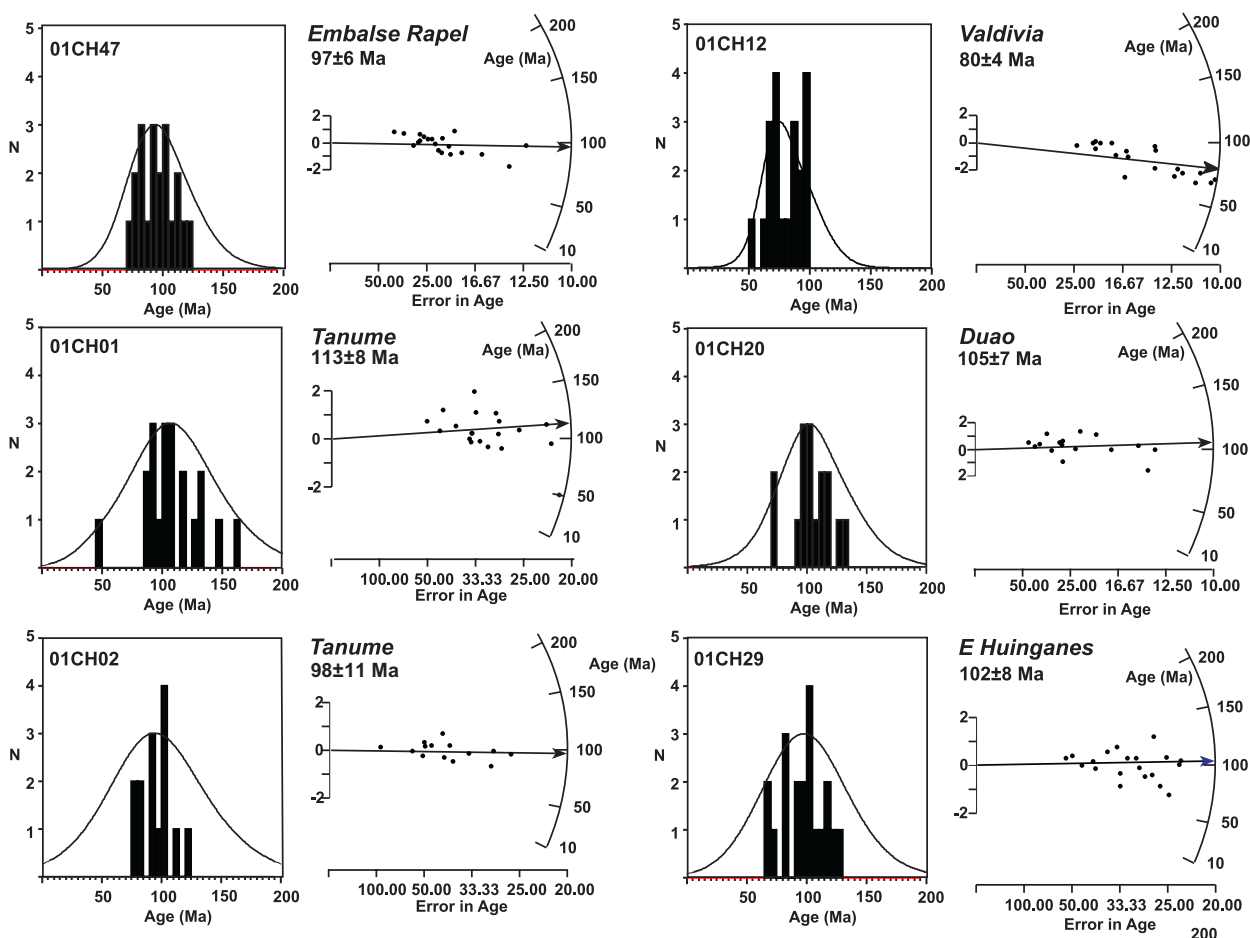

Fig. 5. Histogram and radial plot representation of the apatite single grain fission-track age data from basement rocks of central Chile (34°–35°30′S). (See Table 4.) In the radial plots, *x*-scale is $1/\sigma$, *y*-scale is $(z - z_0)/\sigma$, and *z*-scale represents the age.
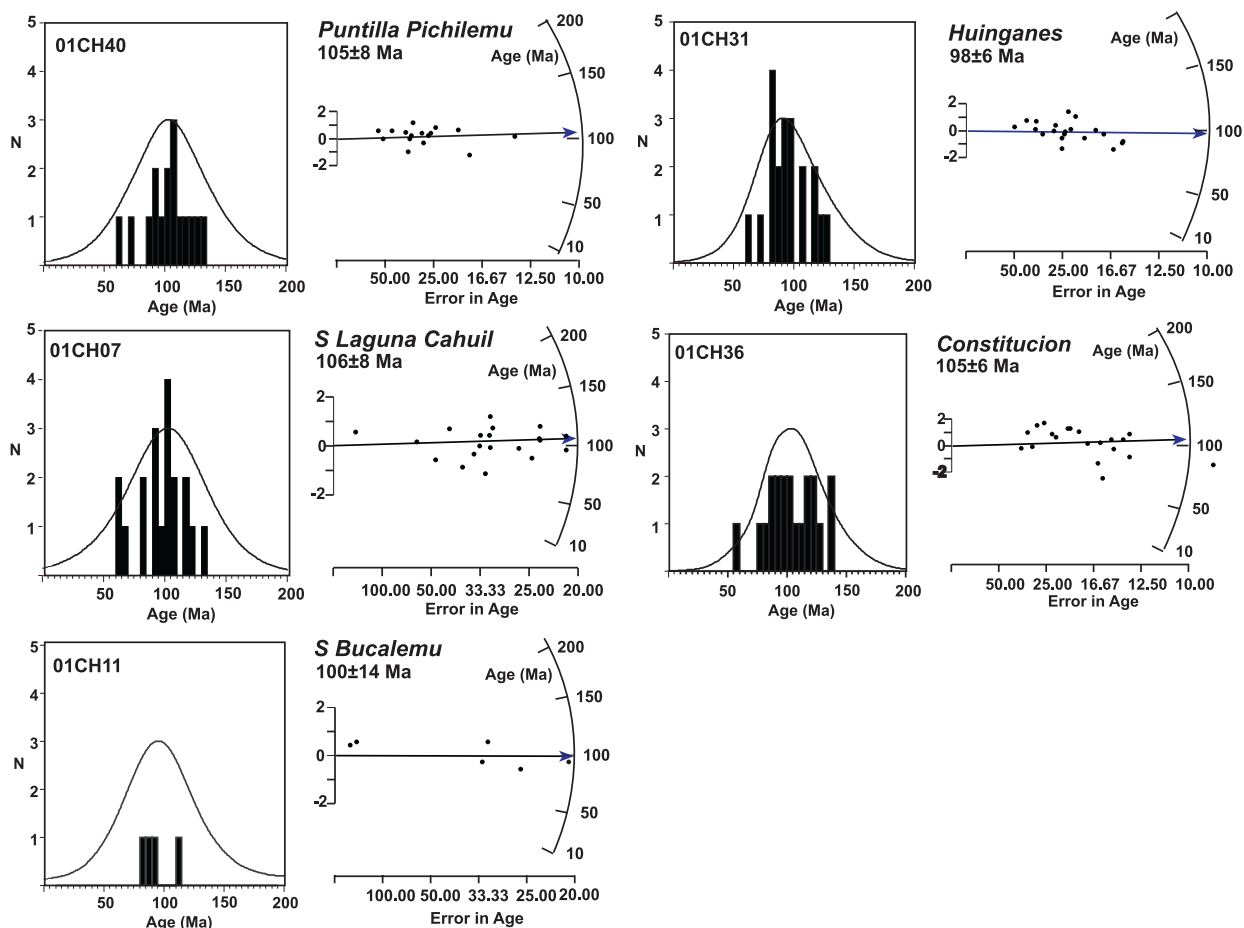
Fig. 5. Continued

DISCUSSION AND GEODYNAMIC IMPLICATIONS

Initiation of the paired metamorphic belt

The depositional ages for both metasedimentary series remain poorly constrained. Hervé (1988) suggested a Devonian to Carboniferous depositional age by correlation with isolated occurrences of macrofossils in northern Chile and on the basis of Rb/Sr errorchron age signatures. Duhart *et al.* (2001) obtained U/Pb single grain ages for the youngest detrital zircons in the Western Series of south–central Chile, indicating maximum depositional ages between 278 Ma and 388 Ma in different samples. Considering the overall setting, deposition of the Eastern Series should have occurred prior to that of the Western Series, because the former rocks were already deformed and metamorphosed when the latter reached their maximum depth in the subduction zone. The rocks of the Eastern Series presumably represent relic sediments of a passive margin that is supposed to have existed during Devonian times before the onset of subduction processes (Hervé, 1988; Bahlburg & Hervé, 1997).

Evidence for the initiation of the subduction process is given by the 'exotic' garnet mica-schist of Punta Sirena that yielded the oldest Ar/Ar white mica age of 320 Ma. Such an interpretation is inferred by analogy with a situation in the Western Series of south–central Chile, where a rare garnet amphibolite represents the highest *PT* conditions, the oldest age of peak metamorphism and an anticlockwise *PT* path (Willner *et al.*, 2004). The garnet mica-schist has the highest recorded *PT* conditions, comparable with those of the garnet amphibolite in south–central Chile, and also provides hints for a similar *PT* evolution (Willner, 2005). The following scenario is suggested during the earliest subduction mass flow according to similar findings in fossil accretionary complexes world wide (Willner *et al.*, 2004, and references therein). At an early stage, material was subducted to great depth and accreted against a hot upper mantle wedge. The early subducted material cooled at depth during continued accretion before being exhumed when a steady-state accretionary prism was established with basal accretion at a moderate depth in front of the mantle wedge. Accretion must have begun slightly earlier than
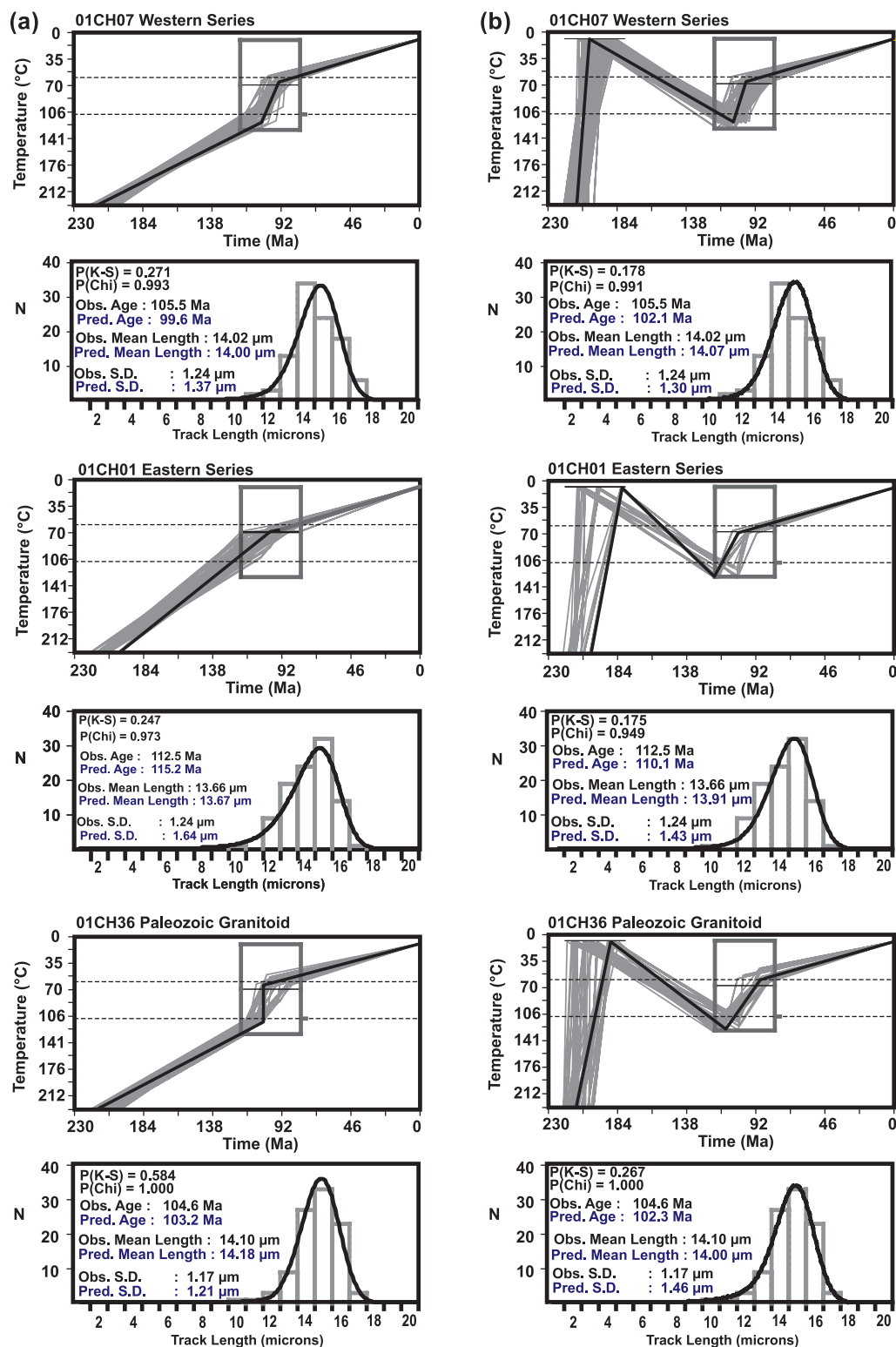
Fig. 6. Modelling of cooling rates on the basis of track length distributions in apatite according to the apatite fission-track annealing model of Laslett *et al.* (1987). The three selected samples (01CH07, 01CH01, 01CH36) cover all basement units in the study area. Alternative models are calculated in the two vertical columns: (a) continuous exhumation; (b) exhumation involving reburial during basin formation. Obs, observed; pred, predicted; S.D., standard deviation; P(Chi) is the χ^2 probability and P(K-S) is the Kolmogorov–Smirnov probability for the goodness of fit between the observed and predicted track length distributions.
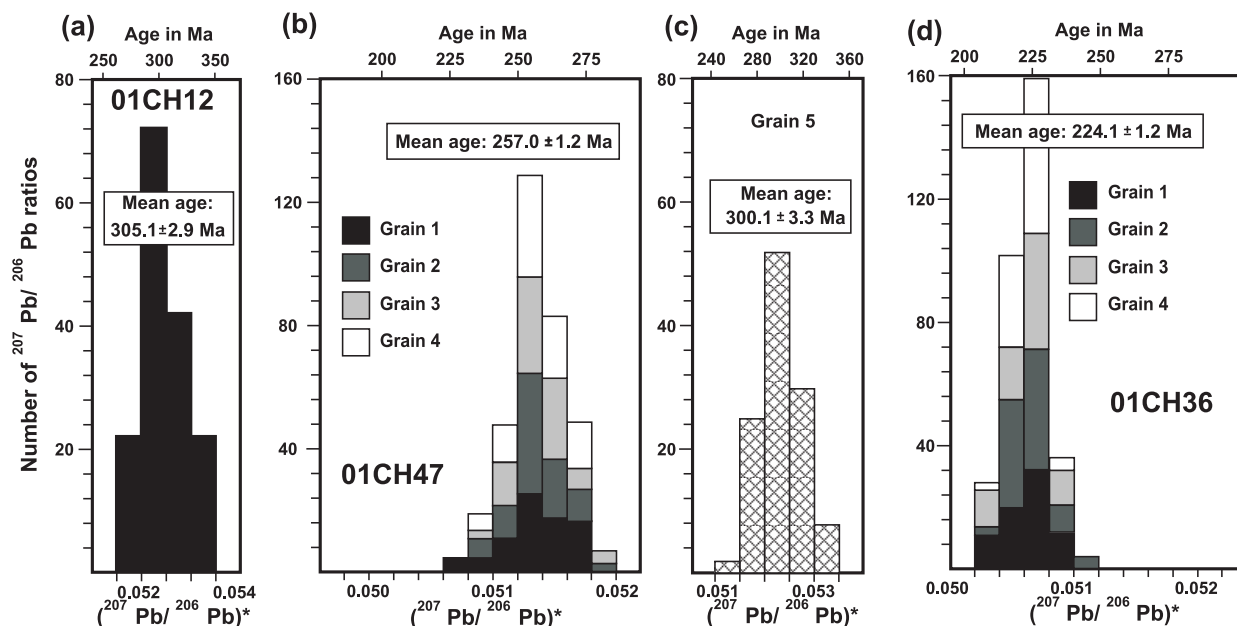
Fig. 7. Histograms showing distribution of radiogenic lead isotope ratios derived from evaporation of zircons from selected granites of the basement in central Chile (34°–35°30′S). (a) Sample 01CH12 (Valdivia): one zircon fraction (four grains). (b) Sample 01CH47 (Central Rapel): spectrum for four grain fractions. (c) Sample 01CH47 (Central Rapel): spectrum for one xenocryst grain. (d) Sample 01CH36 (Constitución): spectrum for four grain fractions. (See Table 5.)

the phengite age of 320 Ma determined in this study, because this phengite grew during an early retrograde stage (Willner, 2005).

The relatively uniform Ar/Ar white mica ages between 296 Ma and 301 Ma in the Eastern Series are in line with the relatively uniform level of HT overprint at ~3 kbar (Willner, 2005) and imply a time-restricted heat input of regional extent. The intrusion age of 305 Ma for the magmatic arc batholith coincides with the range of Rb–Sr isochron granitoid ages of 292–312 Ma north and south of the study area (Hervé *et al.*, 1988). We consider that the narrow age range for the HT metamorphism in the Eastern Series corresponds to the time of major intrusive activity within the late Palaeozoic arc at this latitude. The early and most deeply subducted siliciclastic material around 320 Ma probably released abundant hydrous fluids to trigger these voluminous melts. Nevertheless, the two Pb/Pb zircon ages for arc granites at 257 Ma and 224 Ma indicate that magmatic activity in the late Palaeozoic arc, and hence a similar setting at the convergent margin, continued into late Triassic times, albeit with decreasing magma volumes. A comparable age pattern for the late Palaeozoic arc was also detected in south–central Chile by Martin *et al.* (1999) and Lucassen *et al.* (2004).

The age range for the HT metamorphism in the Eastern Series also falls into the time bracket established for the peak of HP metamorphism in the Western Series at 292–320 Ma. Therefore, a true contemporaneous paired metamorphic belt has been identified for the first time in central Chile. The variable peak metamorphic ages in the Western Series covering a time span of 28 Myr, in contrast to the restricted age range of the Eastern Series, are thought to reflect continuous basal accretion, which is now partially represented by the exposed rocks.

Exhumation period I during continuous accretion

Differences in the evolution of both metamorphic belts become apparent when exhumation rates are compared. If the ^{40}Ar/^{39}Ar white mica plateau ages are accepted as formation ages at peak metamorphic conditions, and the FT ages as cooling ages below 280°C (zircon) and 110°C (apatite), three time markers related to stages along the *PT* trajectory define two periods of contrasting exhumation rates in both series. Depth and temperature for the first time marker were obtained from the peak *PT* data derived from mineral equilibria (Willner, 2005). Depth estimates for the time of closure at the 280°C and 110°C isotherms were made on the following basis.

(1) Because the zircon FT ages are uniform in both metamorphic series and the granites, the corresponding pressure must have been below the peak pressure of the HT metamophism in the Eastern Series (i.e. <3 kbar).

(2) Thermometric estimates in the Mesozoic cover sediments by Belmar *et al.* (2002) indicate a gradient of ≥35°C/km during formation of the Mesozoic

Table 5: Isotopic data from evaporation of zircon from the Chilean metamorphic basement between 34° and 35°30′S

	Mass scans[*]	Evaporation temp. (°C)	Mean $^{207}Pb/^{206}Pb$ ratio[†] and 2σ error	$^{207}Pb/^{206}Pb$ age and 2σ error
Sample 01CH12 (clear, long, euhedral)				
Grain 1[‡]	158	1596	0·052451 ± 67	305·1 ± 2·9
Sample 01CH36 (light yellow–brown, long-prismatic, euhedral)				
Grain 1[‡]	76	1594	0·050617 ± 41	223·5 ± 1·9
Grain 2[‡]	85	1596	0·050624 ± 27	223·8 ± 1·2
Grain 3[‡]	82	1595	0·050648 ± 45	224·9 ± 2·0
Grain 4[‡]	86	1596	0·050631 ± 24	224·1 ± 1·1
Mean of 4 analyses, grains 1—4	329		0·050630 ± 17	224·1 ± 1·2[§]
Sample 01CH47 (clear to light, yellow–brown, long-prismatic, euhedral)				
Grain 1[‡]	82	1596	0·051360 ± 61	257·1 ± 2·7
Grain 2[‡]	87	1588	0·051354 ± 44	256·8 ± 2·0
Grain 3[‡]	85	1605	0·051371 ± 49	257·5 ± 2·2
Grain 4[‡]	85	1585	0·051375 + 48	257·7 ± 2·2
Mean of 4 analyses, grains 1—4	339		0·051365 ± 25	257·3 ± 1·2[§]
As above, large grain, grain 5	117	1599	0·052335 ± 75	300·1 ± 3·3

[*]Number of $^{207}Pb/^{206}Pb$ ratios evaluated for age assessment.
[†]Observed mean ratio corrected for non-radiogenic Pb where necessary. Errors based on uncertainties in counting statistics.
[‡]Grain fraction with 3—4 small grains each.
[§]Error based on reproducibility of internal standard.
Evaporation of zircon fractions was undertaken according to Kober (1986, 1987) with modifications (Kröner & Hegner, 1998). Data acquisition was on a Finnigan-MAT 261 mass spectrometer at Max-Planck-Institut für Chemie in Mainz by magnetic peak switching, using the Secondary Electron Multiplier. No correction was made for mass fractionation of Pb, which is estimated at 0·3‰ per atomic mass unit. Evaporation temperatures were gradually raised in 30—50°C steps during repeated evaporation—precipitation cycles until no further changes in the $^{207}Pb/^{206}Pb$ ratios were observed. Only data from the high-temperature runs or those with no changes in the Pb-isotope ratios were considered. Common Pb corrections followed the model of Stacey & Kramers (1975). Mean ages and errors for several fractions from the same sample are presented as weighted means of the entire population. Principally all $^{207}Pb/^{206}Pb$ ages determined by the evaporation method are minimum ages. These data are likely to represent crystallization ages when (1) the $^{207}Pb/^{206}Pb$ ratio does not change with rising temperature of evaporation and/or (2) repeated analysis of grains from the same sample at high evaporation temperature yields the same isotope ratios within error. Comparative studies with conventional and ion-microprobe U—Pb dating have shown that this assumption is correct (e.g. Kröner *et al.*, 2001, and references therein).

Vichuquén and Hualañé basins that overlie the basement in its eastern part. From this gradient maximum depths of 8 km and 3 km can be derived for the 280°C and 110°C isotherms, respectively.

(3) The maximum depth of 8 km for the 280°C isotherm is consistent with the following observations: (a) the formation of a narrow 100 m wide contact metamorphic zone with biotite, muscovite and cordierite (no garnet) around the Constitución granite (Godoy, 1970), which yielded a Pb/Pb age of 224 Ma; (b) pressures of ≤2·5 kbar as shown by hydrous fluid inclusion isochores in Western Series rocks of south–central Chile (Willner *et al.*, 2001).

Uncertainties in the estimation of depth of metamorphism and age lead to relatively wide-ranging estimates of exhumation rates. Ignoring the garnet mica-schist at Punta Sirena, the duration of cooling from peak temperature in the Western Series (~350–400°C) at depths of ~25–40 km (~7–11 kbar; calculated on the basis of a mean rock density of 2·8 g/cm^3) to 280°C at a depth of ≤8 km would have lasted 62–95 Myr. This translates to an integrated mean exhumation rate of ≥0·19–0·56 mm/yr and a mean cooling rate of ~0·7–1·9°C/Myr for the post-peak metamorphism exhumation period I of the Western Series. Only for the blueschist locality at Pichilemu (Fig. 1) could both bracketing ages and a *PT* estimate of 10·6 kbar, 350°C (Willner, 2005) be derived from the same locality, translating to a mean exhumation rate of 0·32–0·48 mm/yr, consistent with the above range. A comparable initial exhumation rate of 0·26–0·45 mm/yr is estimated for the 'exotic' garnet mica-schist at Punta Sirena with the oldest age and the highest recorded peak *PT* values, if a nearby zircon FT age is taken into consideration. If the range of single white mica ages derived by *in situ* Ar/Ar laser ablation reflects a duration of 32–44 Myr of continuous retrograde mineral growth, then this would

correspond to a mean pressure release of 3–4 kbar (Willner, 2005). This results in a comparable, independently derived exhumation rate of 0·28–0·47 mm/yr.

The initial exhumation rates in the Western Series are relatively low compared with rates in accretionary prisms such as Crete (minimum rate of 4 mm/yr), where tectonic unroofing caused the majority of the overall exhumation of the HP–LT rocks (Thomson *et al.*, 1998). The long-term average exhumation rates in central Chile are only an order of magnitude higher than general mean erosion rates of 0·05 mm/yr, although higher erosion rates of 4 mm/yr or even 13 mm/yr have been recorded in tectonically active, high-relief and wet eroding areas (Ring *et al.*, 1999). Ductile normal faulting is very rare and brittle normal faulting is absent in central Chile. Therefore erosion is assumed to be an important exhumation mechanism for the Western Series. Erosion of an emergent forearc high as a principal exhumation mechanism with inferred erosion rates of 0·4–0·8 mm/yr was implied by Ring & Brandon (1999) for the Franciscan subduction complex, where ductile thinning following basal accretion contributed up to only 10% of the entire exhumation. This also appears to be represented by the penetrative subhorizontal transposition foliation in central Chile, and is the only visible tectonic contribution to exhumation in the Western Series except for rare shear bands. In analogue models of accretionary wedges (Kukowski *et al.*, 2002), the area of the coupling zone where basal accretion takes place has been shown to be the area of principal crustal thickening and topographic elevation. Hence during the recorded period of exhumation in the Western Series a forearc high must be envisaged undergoing continuous erosion balanced by continuous accretion at depth. Hence continuous accretion is indirectly recorded in the rocks of the Western Series for a time span of ∼65 Myr between the oldest peak *PT* and the youngest retrograde mineral formation age.

In contrast, however, exhumation from peak metamorphic conditions in the Eastern Series at 11 km depth (∼3 kbar) to the level of the 280°C isotherm lasted 57–100 Myr and translates into an exhumation rate of 0·03–0·05 mm/yr for exhumation period I, which is one order of magnitude lower than in the Western Series. The low exhumation rates and the scarcity of post-metamorphic deformation after 300 Ma indicate little crustal thickening and a rather long period of stability of the crust in the retro-wedge, in contrast to continuous accretion in the Western Series at the same time. The lack of notable crustal thickening in the late Palaeozoic magmatic arc is remarkable, as a significant crustal component within the intruding magmas was detected (Hervé *et al.*, 1988; Lucassen *et al.*, 2004).

Our data may be compared with those derived from the basement in south–central Chile at 37–42°S (Glodny *et al.*, 2005): systematic Rb–Sr dating of minerals related to specific deformation stages during exhumation yielded a mean exhumation rate of 0·5–0·7 mm/yr, slightly higher than in our study area. This is consistent with ages of the peak of metamorphism being considerably younger than in north–central Chile (∼285 to 233 Ma along a north–south trend), whereas accretion ceased at ∼215 Ma as in north–central Chile. The initiation of accretion is slightly younger in south–central Chile, as shown by the most deeply subducted material, which records an anticlockwise *PT* trajectory and a retrograde blueschist stage at 304 Ma (Willner *et al.*, 2004). The youngest detrital zircon in the basement of south–central Chile was dated at 275 Ma (U/Pb single zircon) by Duhart *et al.* (2001), and must have been incorporated into the accretionary prism a considerable time after initiation of accretion. This strongly corroborates the cyclic nature of the subduction mass flow.

Exhumation period II and the change of geodynamic conditions

A second exhumation period II (∼232–98 Ma) corresponds to cooling between the 280°C and 110°C isotherms, and exhumation from ≤8 to ≤3 km lasted for ∼89–134 Myr over the entire region. This is equivalent to an integrated mean exhumation rate of ≤0·04–0·06 mm/yr and a mean cooling rate of ∼1·3–1·9°C/Myr. This is comparable with the initial post-peak metamorphic cooling and exhumation rates for the Eastern Series. However, for the Western Series a decrease in exhumation rates by a factor of 10 implies a considerable change in the geotectonic framework. The exhumation rates for both series during the exhumation period II are lower than the mean erosion rates of 0·05 mm/yr (Ring *et al.*, 1999). This remarkable drop in exhumation rates between exhumation period I and II indicates that the Western Series was no longer a tectonically active region and implies that accretion ceased after ∼206 Ma. The 224 Ma intrusion age of the Constitución granite into the Western Series sets another time limit for the end of basal accretion. Zircon FT ages in the southern part of the study area are remarkably similar to that age. Therefore, detectable accretion activity as a result of long-term basal underplating in the accretionary prism in central Chile lasted for ∼100 Myr during the interval 320–224 Ma. After this time the late Palaeozoic accretion system remained inactive despite continuing subduction at the convergent margin.

According to Charrier (1979) and Thiele & Morel (1981), tectonic development during the late Triassic and Jurassic was controlled by continuous extensional movements and differential uplift of the surrounding basement areas, resulting in a simple morphology of locally subsiding basins and broad rising elevations.

The oldest zircon FT ages in the basement coincide with the time of deposition of the oldest clastic sediments in the eastern part of the exposed basement (~220 Ma; Corvalán, 1976). Younger zircon FT ages of 206 and 207 Ma in the north of our study area may be related to the opening of early Jurassic basins in the Vichuquén area. Diagenesis in these basins was dated at 206 Ma (K–Ar illite) by Belmar et al. (2004). In this region cooling may have been retarded by reburial of the basement in the vicinity of the basins. Nevertheless, most of the now exposed basement was undergoing continued erosion as indicated by abundant Upper Triassic to Lower Jurassic siliciclastic sedimentary rocks of proximal provenance in the surrounding basins, implying the existence of a certain surface relief in nearby areas (Belmar et al., 2002). Two possible alternative scenarios are envisaged following the cessation of accretion: (1) rapid cooling and exhumation to the surface after 220 Ma and reburial to very low-grade metamorphic conditions or (2) continuous slow cooling and exhumation between 232 and 98 Ma. Distinction between these scenarios cannot be made on the basis of FT data alone. The palaeogeographical situation requires a combination of the two models, and the Ar/Ar age spectrum of the Jurassic magmatic microcline supports the second alternative.

The remarkably long time interval of 89–134 Myr between zircon and apatite FT closure indicates a long period of relative crustal stability. This interval corresponds to the time of formation of marine basins in central Chile, including the area of the magmatic arc, and is interpreted as a period of major extension (Thiele & Morel, 1981; Charrier & Muñoz, 1994). An extensional fore-arc setting during the Jurassic for the basement of the study area is reflected by the 138 Ma rhyolite dyke age that is part of an abundant bimodal association of late post-tectonic basaltic and rhyolitic dykes. The exotic zircon FT age of 142 Ma may be interpreted as reflecting a localized near-surface reheating event during the Jurassic fore-arc magmatism.

Basins opened in late Triassic times along a NNW–SSE trend joining an en échelon pattern with rift basins in Argentina (Ramos & Mahlburg Kay, 1991). In the Coastal Cordillera north of Santiago (30–33°S), abundant bimodal magmatism in late Triassic to early Jurassic times contrasts with later calc-alkaline plutonism in the Mesozoic arc (Parada et al., 1991) reflecting major extension and crustal thinning. The modern Andean arc began to develop along the central Chilean margin during mid-Jurassic times. However, the extensional regime extended into the intracratonic region during most of the Jurassic and early Cretaceous with formation of new marine intra-arc basins in a north–south direction (Charrier & Muñoz, 1994).

The end of accretion within the Western Series after ~224 Ma may be caused by a retreat of the subducting slab as implied by the late Triassic intrusions into the Western Series, but also, for the following reasons, by an associated lack of detritus supply:

(1) surface relief in the Mesozoic extensional terrain was probably less pronounced than in the late Palaeozoic active convergent regime, resulting in slower erosion rates;

(2) substantial accumulation of detritus during the Mesozoic mainly occurred in actively subsiding intracontinental basins rather than in the trench;

(3) a change in climate may have caused a further decrease in detritus supply. Charrier (1988) summarized evidence for a cold humid climate in central Chile during late Palaeozoic times. By contrast, the continental hinterland became more arid during late Triassic times and, during most of the Mesozoic, warm climatic conditions prevailed (Charrier & Muñoz, 1994).

Exhumation periods III and IV

The high cooling rates of ≥ 3–$5°C$/Myr at ~115–90 Ma derived from apatite FT modelling correspond to exhumation rates of 0·08–0·14 mm/yr. Such rates are significantly higher than the long-term average cooling rates derived from all basement rocks for exhumation period II. The mid-Cretaceous increase in cooling and, hence, exhumation rate (exhumation period III) may be interpreted as a return to convergent tectonic conditions in the light of the following regional observations.

Parada & Larrondo (1999) and Gana & Zentilli (2000) obtained apatite FT ages of a similar age range (91–106 Ma) from the Coastal Cordillera, west of Santiago, about 100–150 km north of our study area. Arancibia (2004) postulated a contractional regime associated with the closure of early Cretaceous basins and an increase in the exhumation–erosion rate in the Coastal Cordillera during mid-Cretaceous time. Arancibia (2004) identified a NNE-striking shear zone with reverse-slip kinematics active at 98–109 Ma (Ar/Ar mica) at Silla del Gobernador, NW of Santiago. This is related to a substantial increase in erosion rate, surface uplift and detritus supply. A change from extension during the Jurassic and early Cretaceous to compression during the mid-Cretaceous with closure of the Mesozoic intra-arc basins was also recognized by Bravo Espinosa (2001) at the latitude of the study area.

By analogy with the regional situation, the calculated mid-Cretaceous acceleration of exhumation rates in our study area could also be related to a mid-Cretaceous age for the prominent Pichilemu–Vichuquén Fault, which partly separates the Western and Eastern Series (Fig. 1). Reverse fault kinematics with a sinistral strike-slip component have been noted by U. Ring (personal communication, 2004) for this late brittle structure. The fault cuts HT metamorphic isograds in the Eastern Series and has
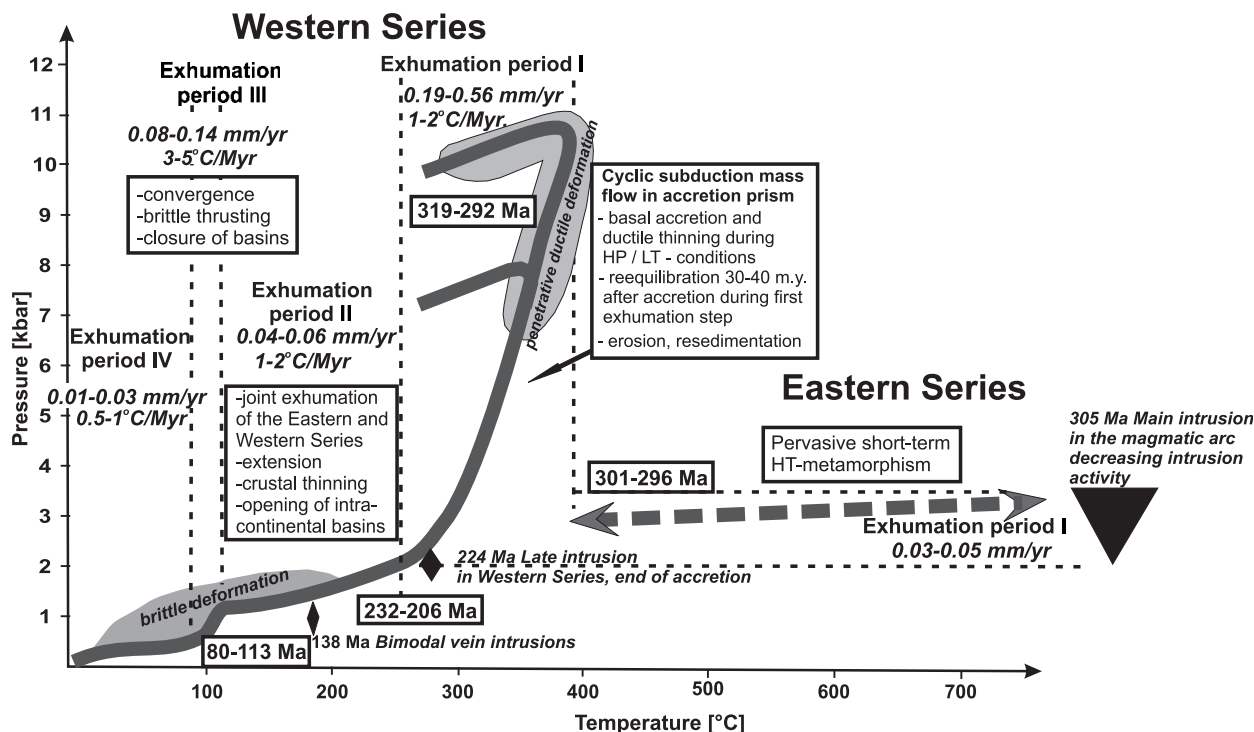
Fig. 8. Summary of the *PT*–time evolution of the late Palaeozoic paired metamorphic belt in central Chile (34°–35°30′S).

an apparent post-metamorphic vertical displacement of a few kilometres.

After 90 Ma, the cooling rates slowed down, with less than 60°C cooling, equivalent to ∼2–3 km of exhumation until today (exhumation period IV). The post-mid-Cretaceous cooling and exhumation rates of 0·5–1°C/Myr and ≤0·03 mm/yr are of the same low magnitude as those that persisted during the exhumation period II.

CONCLUSIONS

Subduction mass flow within an accretionary system was active throughout central Chile between ∼320 and 224 Ma associated with the development of a coeval magmatic arc. Similar accretion activity has not been described at this latitude either before or after this period and thus it represents a time-restricted period of crustal growth. The evolution of the paired metamorphic belt can be summarized as follows (Fig. 8).

After a presumably passive margin stage before late Carboniferous times accretion began shortly before ∼320 Ma, when siliciclastic rocks were most deeply subducted against a still hot mantle wedge. At ∼305 Ma the bulk of late Palaeozoic arc magmas were intruded, presumably triggered by dehydration of the early subducted material. At the same time, and after their main deformation stage, rocks of the Eastern Series were overprinted by a short-term, but pervasive, HT metamorphism at

301–296 Ma. Coarse phengite grains from strain-free domains in exposed rocks of the Western Series show Ar/Ar plateau ages of 320–292 Ma, which are interpreted as mineral formation ages reflecting peak HP–LT metamorphic conditions.

Ar/Ar UV laser ablation ages of phengite grains in well-defined structural positions reveal an age range of 31–41 Myr on a thin-section scale, beginning with the oldest ages equivalent to the coarse phengite Ar/Ar plateau ages. No age relationship with deformation intensity was detected. Pervasive deformation represented by ductile thinning following basal accretion must have ended shortly after peak metamorphic conditions. The Ar/Ar laser ablation ages of phengite reflect new growth and recrystallization during decompression by 3–4 kbar with accretion continuing at depth.

At 224 Ma a late post-tectonic granite intruded into the Western Series, indicating termination of accretion and a retreat of the subducting slab. At the same time, zircon FT ages of 232–206 Ma mark cooling below the 280°C isotherm. Hence, mean exhumation rates of ≥0·19–0·56 mm/yr (exhumation period I) during continuing accretion—combined with a lack of substantial retrograde extensional deformation—suggest that exhumation was mainly controlled by erosion of a tectonically active region. The retro-wedge area is represented by the Eastern Series and was exhumed at rates of 0·03–0·05 mm/yr during the same period, indicating very little crustal

thickening and tectonic activity. The *PT*–time evolution of the exposed rocks of the Western Series points towards a cyclic subduction mass flow during a uniform period of accretion in central Chile, involving continuous accretion, erosion-controlled exhumation, erosion and re-sedimentation in the trench.

After the end of accretion, exhumation rates decreased to ≤0·04–0·06 mm/yr until 113–80 Ma (exhumation period II), when apatite FT ages indicate cooling through the 110°C isotherm. The period from late Triassic to early Cretaceous times was characterized by extension, crustal thinning and formation of intracontinental basins, also in the intra-arc area. Bimodal dyke intrusions in the basement at ∼138 Ma point to extension in the Jurassic fore-arc. Whereas exhumation period II was characterized by cooling rates of ∼1–2°C/Myr, an acceleration to 3–5°C/Myr becomes notable in mid-Cretaceous times, corresponding to an increased exhumation rate of 0·08–0·14 mm/yr (exhumation period III). Renewed convergence caused closure of basins, prominent brittle thrusting in the basement and shortening of the continental margin. After this short event, exhumation and cooling rates again slowed down to average rates of 0·5–1°C/Myr and ≤0·03 mm/yr (exhumation period IV).

ACKNOWLEDGEMENTS

SUPPLEMENTARY DATA

Supplementary data for this paper are available on *Journal of Petrology* online.

REFERENCES

Aguirre, L., Hervé, F. & Godoy, E. (1972). Distribution of metamorphic facies in Chile: an outline. *Krystallinikum* **9**, 7–19.

Arancibia, G. (2004). Mid-Cretaceous crustal shortening: evidence from a regional-scale ductile shear zone in the Coastal Range of central Chile (32°S). *Journal of South American Earth Sciences* **17**, 209–226.

Bahlburg, H. & Hervé, F. (1997). Geodynamic evolution and tectono-stratigraphic terranes of northwestern Argentina and northern Chile. *Geological Society of America Bulletin* **109**, 869–884.

Belmar, M., Schmidt, S. T., Ferreiro Mählmann, R., Mullis, J., Stern, W. B. & Frey, M. (2002). Diagenesis, low-grade and contact metamorphism in the Triassic–Jurassic of the Vichuquén–Tilicura and Hualañé–Gualleco Basins, Coastal Range of Chile. *Schweizerische Mineralogische und Petrographische Mitteilungen* **82**, 375–392.

Belmar, M., Morata, D., Munizaga, F., Pérez de Arce, C., Morales, S. & Carrillo, F. J. (2004). Significance of K–Ar dating of very low-grade metamorphism in Triassic–Jurassic pelites from the Coastal Range of central Chile. *Clay Minerals* **39**, 151–162.

Bravo Espinosa, P. J. (2001). Geologia del borde oriental de la Cordillera de la Costa entre los rios Mataquito y Maule, VII región. M.Sc. thesis, Universidad de Chile, Santiago, 113 pp.

Brix, M. R., Stöckhert, B., Seidel, E., Theye, T., Thomson, S. N. & Küster, M. (2002). Thermobarometric data from a fossil zircon partial annealing zone in high pressure–low temperature rocks of eastern and central Crete, Greece. *Tectonophysics* **349**, 309–326.

Charrier, R. (1979). El Triásico en Chile y regione adyacentes de Argentina: una reconstrucción paleogeográfica y paleoclimatica. *Communicaciones* **26**, 1–37.

Charrier, R. (1988). Condiciones paleoclimáticas para el Carbonífero superior y Permico inferior en la mitad Austral de America del Sur. *Boletin del Museo Nacional de Historia Natural de Chile* **41**, 105–116.

Charrier, R. & Muñoz, N. (1994). Jurassic–Cretaceous paleogeographic evolution of the Chilean Andes at 23°–24° and 34°–35°S latitude: a comparative analysis. In: Reutter, K.-J., Scheuber, E. & Wigger, P. (eds) *Tectonics of the Southern Central Andes*. Berlin: Springer, pp. 233–242.

Cordani, U., Munizaga, F., Hervé, F. & Hervé, M. (1976). Edades radiométricas provenientes del Basamento Cristalino de la Cordillera de la Costa de las Provincias de Valparaiso y Santiago, Chile. *Actas I Congreso Geológico Chileno, Santiago* **2**, F213–F222.

Corvalán, J. (1976). El Triásico y Jurasico de Vichuquén–Tilicura y de Hualañé, Provincia de Curico. Implicaciones paleogeograficas. *Actas I Congreso Geológico Chileno, Santiago* **1**, A137–A154.

Cowan, D. S. & Schilling, R. M. (1978). A dynamic scaled model of accretion at trenches and its implications for the tectonic evolution of subduction complexes. *Journal of Geophysical Research* **83**, 5389–5396.

Dávila, A., Hervé, F. & Munizaga, F. (1979). Edad K–Ar en granitoides de la Cordillera de la Costa de la provincia de Colchagua, VII Región, Chile Central. *Actas II Congreso Geológico Chileno* F109–F120.

De Jong, K., Féraud, G., Ruffet, G., Amouric, M. & Wijbrans, J. R. (2001). Excess argon incorporation in phengite of the Mulhacén Complex: submicroscopic illitization and fluid ingress during late Miocene extension in the Betic Zone, south-eastern Spain. *Chemical Geology* **178**, 159–195.

Duhart, P., McDonough, M., Muñoz, J., Martin, M. & Villeneuve, M. (2001). El complejo metamórfico Bahía Mansa en la Cordillera de la Costa del centro-sur de Chile (39°30′–42°00′S): geocronología K–Ar, ^{40}Ar/^{39}Ar y U–Pb e implicancias en la evolución del margen sur-occidental de Gondwana. *Revista Geologica de Chile* **28**, 179–208.

Ernst, W. G. (1975). Systematics of large-scale tectonics and age progressions in Alpine and Circum-Pacific blueschist belts. *Tectonophysics* **26**, 229–246.

Galbraith, R. F. (1990). The radial plot: graphical assessment of spread in ages. *Nuclear Tracks and Radiation Measurements* **17**, 207–214.

Galbraith, R. F. & Laslett, G. M. (1993). Statistical models for mixed fission track ages. *Nuclear Tracks and Radiation Measurements* **21**, 459–470.

Gallagher, K. (1995). Evolving temperature histories from apatite fission-track data. *Earth and Planetary Science Letters* **136**, 421–435.

Gana, P. & Hervé, F. (1983). Geologia del basamento cristalino en la Cordillera de la Costa entre los rios Mataquito y Maule, VII region. *Revista Geologica de Chile* **19–20**, 37–56.

Gana, P. & Zentilli, M. (2000). Historia termal y exhumación de intrusivos de la Cordillera de la Costa de Chile central. *Actas IX Congreso Geológico Chileno* **2**, 664–668.

Gerya, T. V., Stöckhert, B. & Perchuk, A. L. (2002). Exhumation of high-pressure metamorphic rocks in a subduction channel—a numerical simulation. *Tectonics* **21**, 6-1–6-19.

Glodny, J., Lohrmann, J., Echtler, H., Gräfe, K., Seifert, W., Collao, S. & Figueroa, O. (2005). Internal dynamics of a paleoaccretionary wedge: insights from combined isotope tectonochronology and sandbox modelling of the South–Central Chilean forearc. *Earth and Planetary Science Letters* **231**, 23–39.

Godoy, E. (1970). Estudio petrográfico del granito de Constitución y su aureola de metamorfismo de contacto. B.Sc. thesis, Universidad de Chile, Santiago, 130 pp.

González Bonorino, F. (1971). Metamorphism of the crystalline basement of central Chile. *Journal of Petrology* **12**, 149–175.

Green, P. F., Duddy, I. R., Laslett, G. M., Hegarty, K. A., Gleadow, A. J. W. & Lovering, J. F. (1989). Thermal annealing of fission tracks in apatite, 4, Quantitative modelling techniques and extension to geological timescales. *Chemical Geology* **79**, 155–182.

Harrison, T. M., Lovera, O. M. & Heitzler, M. T. (1991). $^{40}Ar/^{39}Ar$ results for alkali feldspars containing multiple diffusion domains with differing activation energy. *Geochimica et Cosmochimica Acta* **55**, 1435–1448.

Hervé, F. (1988). Late Paleozoic subduction and accretion in Southern Chile. *Episodes* **11**, 183–188.

Hervé, F., Munizaga, F., Godoy, E. & Aguirre, L. (1974). Late Paleozoic K–Ar ages of blueschists from Pichilemu, central Chile. *Earth and Planetary Science Letters* **23**, 261–264.

Hervé, F., Munizaga, F., Mantovani, M. & Hervé, M. (1976). Edades de Rb–Sr neopaleozoicas del Basamento Cristalino de la Cordillera de Nahuelbuta. *Actas I Congreso Geológico Chileno, Santiago* **2**, F19–F26.

Hervé, F., Kawashita, K., Munizaga, F. & Bassei, M. (1984). Rb–Sr isotopic ages from late Paleozoic metamorphic rocks of Central Chile. *Journal of the Geological Society, London* **141**, 877–884.

Hervé, F., Munizaga, F., Parada, M. A., Brook, M., Pankhurst, R. J., Snelling, N. J. & Drake, R. (1988). Granitoids of the coast range of central Chile: geochronology and geologic setting. *Journal of South American Earth Sciences* **1**, 185–194.

Hurford, A. J. (1990). Standardization of fission track dating calibration: recommended by the Fission Track Working Group of the I.U.G.S. Subcommission on Geochronology. *Chemical Geology, Isotope Geoscience Section* **80**, 171–178.

Hurford, A. J. & Green, P. F. (1983). The zeta age calibration of fission-track dating. *Isotope Geoscience* **1**, 285–317.

Hurford, A. J., Hunziker, J. C. & Stöckhert, B. (1991). Constraints on the late thermotectonic evolution of the western Alps: evidence for episodic rapid uplift. *Tectonics* **10**, 758–769.

Ketcham, R. A., Donelick, R. A. & Carlson, W. D. (1999). Variability of apatite fission-track annealing kinetics: III. Extrapolation to geological time scales. *American Mineralogist* **84**, 1235–1255.

Kober, B. (1986). Whole-grain evaporation for $^{207}Pb/^{206}Pb$-age investigations on single zircons using a double-filament thermal ion source. *Contributions to Mineralogy and Petrology* **93**, 482–490.

Kober, B. (1987). Single-zircon evaporation combined with Pb + emitter-bedding for $^{207}Pb/^{206}Pb$-age investigations using thermal ion mass spectrometry, and implications to zirconology. *Contributions to Mineralogy and Petrology* **96**, 63–71.

Kröner, A. & Hegner, E. (1998). Geochemistry, single zircon ages and Sm–Nd systematics of granitoid rocks from the Góry Sowie (Owl) Mts., Polish West Sudetes: evidence for early Paleozoic arc-related plutonism. *Journal of the Geological Society, London* **155**, 711–724.

Kröner, A., Willner, A. P., Hegner, E., Jaeckel, P. & Nemchin, A. (2001). Single zircon ages, *PT* evolution and Nd isotopic systematics of high-grade gneisses in southern Malawi and their bearing on the evolution of the Mozambique belt in southeastern Africa. *Precambrian Research* **109**, 257–291.

Kukowski, N., Lallemand, S. E., Malavieille, J., Gutscher, M.-A. & Reston, T. J. (2002). Mechanical decoupling and basal duplex formation observed in sandbox experiments with application to the Western Mediterranean Ridge accretionary complex. *Marine Geology* **186**, 29–42.

Laslett, G. M., Green, P. F., Duddy, I. R. & Gleadow, A. J. W. (1987). Thermal annealing of fission tracks in apatite: 2. A quantitative analysis. *Chemical Geology, Isotope Geoscience Section* **65**, 1–13.

Lucassen, F., Trumbull, R., Franz, G., Creixell, C., Vásquez, P., Romer, R. L. & Figueroa, O. (2004). Distinguishing crustal recycling and juvenile additions at active continental margins: the Paleozoic to recent compositional evolution of the Chilean continental margin (36°–41°S). *Journal of South American Earth Sciences* **17**, 103–119.

Martin, M. W., Kato, T. T., Rodriguez, C., Godoy, E., Duhart, P., McDonough, M. & Campos, A. (1999). Evolution of the late Paleozoic accretionary complex and overlying forearc–magmatic arc, south central Chile (38°–41°S): constraints for the tectonic setting along the southwestern margin of Gondwana. *Tectonics* **18**, 582–605.

McDougall, I. & Harrison, T. M. (1999). *Geochronology and Thermochronology by the $^{40}Ar/^{39}Ar$ Method*. Oxford: Oxford University Press, 269 pp.

Parada, M. & Larrondo, P. (1999). Thermochronology of the Lower Cretaceous Caleu Pluton in the coastal range of central Chile: tectonostratigraphic implications. *Abstracts, 4th International Symposium of Andean Geodynamics, Göttingen*, pp. 563–566.

Parada, M. A., Levi, B. & Nystrom, J. O. (1991). Geochemistry of the Triassic to Jurassic plutonism of central Chile (30 to 33°S); petrogenetic implications and a tectonic discussion. In: Harmon, R. S. & Rapela, C. W. (eds) *Andean Magmatism and its Tectonic Setting. Geological Society of America, Special Papers* **265**, 99–112.

Rahn, M. K., Brandon, M. T., Batt, G. E. & Garver, J. I. (2004). A zero-damage model for fission-track annealing in zircon. *American Mineralogist* **89**, 473–484.

Ramos, V. A. & Mahlburg Kay, S. (1991). Triassic rifting and associated basalts in the Cuyo basin, central Argentina. In: Harmon, R. S. & Rapela, C. W. (eds) *Andean Magmatism and its Tectonic Setting. Geological Society of America, Special Papers* **265**, 79–91.

Ring, U. & Brandon, M. T. (1999). Ductile deformation and mass loss in the Franciscan subduction complex: implications for exhumation processes in accretionary wedges. In: Ring, U., Brandon, M. T., Lister, G. S. & Willett, S. D. (eds) *Exhumation Processes: Normal Faulting, Ductile Flow and Erosion. Geological Society, London, Special Publications* **154**, 55–86.

Ring, U., Brandon, M. T., Willett, S. D. & Lister, G. S. (1999). Exhumation processes. In: Ring, U., Brandon, M. T., Lister, G. S. & Willett, S. D. (eds) *Exhumation Processes: Normal Faulting, Ductile Flow and Erosion. Geological Society, London, Special Publications* **154**, 1–27.

Shibata, K., Ishihara, S. & Ulrikson, C. (1984). Rb–Sr ages and initial $^{87}Sr/^{86}Sr$ ratios of late Paleozoic granitic rocks from northern Chile. *Bulletin of the Geological Survey of Japan* **25**, 537–545.

Stacey, J. S. & Kramers, J. D. (1975). Approximation of terrestrial lead isotope evolution by a two stage model. *Earth and Planetary Science Letters* **6**, 15–25.

Steiger, R. J. & Jäger, E. (1977). Subcommission on geochronology: convention on the use of decay constants in geo- and cosmochronology. *Earth and Planetary Science Letters* **36**, 359–362.

Tagami, T., Galbraith, R. F., Yamada, R. & Laslett, G. M. (1998). Revised annealing kinetics of fission tracks in zircon and geological implications. In: Van den Haute, P. & De Corte, F. (eds) *Advances in Fission-Track Geochronology*. Dordrecht: Kluwer Academic, pp. 99–112.

Thiele, R. C. & Morel, G. (1981). Tectonica Triásico-Jurásica en la Cordillera de la Costa al norte y sur del Rio Mataquito (34°45′–35°15′ lat. S). *Revista Geológica de Chile* **13–14**, 49–61.

Thomson, S. N., Stöckhert, B. & Brix, M. R. (1998). Thermochronology of the high-pressure metamorphic rocks of Crete, Greece: implications for the speed of tectonic processes. *Geology* **26**, 259–262.

Villa, I. M. (1998). Isotopic closure. *Terra Nova* **10**, 42–47.

Wijbrans, J. R. & McDougall, I. (1986). $^{40}Ar/^{39}Ar$ dating of white micas from an Alpine high-pressure belt on Naxos (Greece): resetting of the argon isotopic system. *Contributions to Mineralogy and Petrology* **93**, 187–194.

Wijbrans, J. R., Pringle, M. S., Koppers, A. A. P. & Scheveers, R. (1995). Argon geochronology of small samples using the VULKAAN argon laser-probe. *Proceedings, Koningklijke Nederlandse Akademie van Wetenschappen* **98**, 185–218.

Willner, A. P. (2005). Pressure–temperature evolution of a Late Palaeozoic paired metamorphic belt in north–central Chile (34°–35°30′S). *Journal of Petrology* **46**, 000–000.

Willner, A. P., Hervé, F. & Massonne, H.-J. (2000). Mineral chemistry and pressure–temperature evolution of two contrasting high-pressure–low-temperature belts in the Chonos Archipelago, Southern Chile. *Journal of Petrology* **41**, 309–330.

Willner, A. P., Pawlig, S., Massonne, H.-J. & Hervé, F. (2001). Metamorphic evolution of spessartine quartzites (coticules) in the high pressure/low temperature complex at Bahia Mansa (Coastal Cordillera of Southern Central Chile). *Canadian Mineralogist* **39**, 1547–1569.

Willner, A. P., Glodny, J., Gerya, T. V., Godoy, E. & Massonne, H.-J. (2004). A counterclockwise *PTt*-path of high pressure–low temperature rocks from the Coastal Cordillera accretionary complex of South Central Chile: constraints for the earliest stage of subduction mass flow. *Lithos* **75**, 283–310.